Surface runoff and sediment yield modelling under no-till: chiselling and crop management effects

Fabio José Andres Schneider, Jean Paolo Gomes Minella, Ana Lúcia Londero, Dinis Deuschle, Gustavo Henrique Merten, Olivier Evrard, Olivier Cerdan, Alice Prates Bisso Dambroz

Hydrological Processes

WILEY

RESEARCH ARTICLE OPEN ACCESS

Surface Runoff and Sediment Yield Modelling Under No-Till: Chiselling and Crop Management Effects

Fabio José Andres Schneider[1] | Jean Paolo Gomes Minella[1] | Ana Lúcia Londero[1] | Dinis Deuschle[1] | Gustavo Henrique Merten[2] | Olivier Evrard[3] | Olivier Cerdan[4] | Alice Prates Bisso Dambroz[1]

[1]Department of Soils, Federal University of Santa Maria, Santa Maria, Brazil | [2]Department of Civil Engineering, University of Minnesota-Duluth, Duluth, Minnesota, USA | [3]Laboratoire Des Sciences et de L'environnement, UMR 8212 (CEA/CNRS/UVSQ-IPSL), Université Paris-Saclay, Gif-sur-Yvette Cedex, France | [4]Risk and Prevention Division, Bureau de Recherches Géologiques et Minières (BRGM), Orléans, France

Correspondence: Fabio José Andres Schneider (fjas.schneider@gmail.com)

Received: 18 April 2025 | **Revised:** 26 November 2025 | **Accepted:** 27 November 2025

Keywords: apparent infiltration | hillslope hydrology | hydrological monitoring | LISEM | no-till agriculture

ABSTRACT

No-till conserves the soil by minimizing disturbance and maintaining crop residue on the surface; however, runoff generation and propagation on no-till hillslopes are not well understood due to the high cost and labor requirements of field monitoring. Hydrological models can help advance this understanding by simulating runoff, sediment yield, and infiltration under different management conditions. This study evaluated the performance of the LISEM model in simulating runoff and sediment yield on hillslopes under no-till agriculture with different soil management practices (with and without chiseling) and cover crop levels, and compared model-simulated infiltration (Green-Ampt method) with apparent infiltration derived from field observations. Rainfall events were monitored from 2014 to 2018 in experimental units of 0.6 ha and 2.5 ha. Nineteen events covering a range of rainfall intensities and seasons were recorded using manual and automatic measurements (2–5 min intervals). LISEM was calibrated and validated for runoff and sediment yield at both spatial scales. For calibration events, Green-Ampt infiltration was directly compared with apparent infiltration estimated from rainfall-runoff data. Model performance was assessed using NSE and PBIAS. Runoff simulations showed good calibration (NSE = 0.99) and satisfactory validation (NSE > 0.5). Sediment yield was well reproduced during calibration but showed lower accuracy in validation, requiring reduced soil cohesion to match observed values. Infiltration simulated by the Green-Ampt method correlated strongly with apparent infiltration (NSE > 0.98), especially at the larger scale, where spatial variability is lower. Overall, the results demonstrate that LISEM can adequately represent runoff processes and infiltration in no-till systems with different management practices and surface cover conditions. The model provides a useful tool for evaluating and designing conservation practices, such as broad-based terraces and retention or detention structures, aimed at mitigating excess runoff and soil loss in agricultural landscapes.

1 | Introduction

No-till is widely adopted worldwide—especially in South America and Brazil—due to its well-documented benefits to soil quality, including increased biological activity, carbon accumulation, water storage, improved structure and fertility, reduced erosion, and enhanced biodiversity (Boddey et al. 2010; Derpsch et al. 2010; Schick et al. 2017; Kassam et al. 2018; Dang et al. 2020; Ferreira et al. 2020; Fuentes-Llanillo et al. 2021; Pott et al. 2023). Crop residues protect the soil surface by reducing raindrop impact and runoff velocity (Merten et al. 2015; Govers et al. 2000; Bradford and Huang 1994). However, intense rainfall, low infiltration rates and saturated or compacted soils can still generate surface runoff capable of detaching soil particles (Londero, Minella, Schneider, et al. 2021, 2021; Qin et al. 2019). At the catchment

scale, runoff propagation is governed by topography and surface roughness (Didoné et al. 2021; Barros et al. 2021; Silva et al. 2021). In Southern Brazil, where long hillslopes and convergent areas enhance runoff energy, disruption of soil cover and rill formation remain widespread even under no-till (Morais and Cogo 2001; Rieke-Zapp and Nearing 2005). Thus, no-till alone is often insufficient to control runoff in steep agricultural landscapes, requiring complementary runoff management practices to mitigate erosion, pollutant transport, and flooding.

Understanding the processes that trigger soil erosion requires long-term, continuous, and often costly monitoring efforts, which provides the field-derived data necessary for model calibration and validation, used for evaluating land and runoff management scenarios (Werle et al. 2025). Hydrological monitoring of no-till agricultural hillslopes is particularly important to assess how precipitation is partitioned between infiltration and surface runoff, the latter being a major driver of soil erosion (Hawkins and Cundy 1987). Infiltration at the soil surface determines the fraction of rainfall that becomes overland flow and is influenced by soil texture, structure, antecedent moisture content, compaction, and land management (dos Santos et al. 2018; Rauber et al. 2025). Although no-till tends to enhance infiltration through residue cover and improved aggregation (Rauber et al. 2025), high spatial and temporal variability requires site-specific monitoring and modelling approaches. Infiltration can be assessed at the point scale using infiltrometers, or inferred at the hillslope or catchment scale through rainfall-runoff relationships, such as apparent infiltration, allowing for an integrated assessment over heterogeneous surfaces (de Barros, Minella, Tassi, et al. 2014; Koppe et al. 2022).

Various empirical and physically based models have been developed to represent infiltration (Assouline 2013). Horton's (1933) empirical model describes the decay of infiltration capacity over time, while physically conceptual models, such as Green and Ampt's (1911), assume a sharp wetting front and accounts for capillary suction and gravitational forces. Despite simplifying assumptions, the Green-Ampt model provides a reasonable balance between physical realism and computational simplicity, and is widely used in hydrological and erosion modelling (Van den Putte et al. 2013; Werle et al. 2025). Accurate representation of infiltration is essential for simulating runoff (and, consequently, sediment transport and nutrient losses) in agricultural catchments, which are therefore used for designing conservation practices that protect soil and water resources (Silva et al. 2021; Werle et al. 2025).

Quantifying these field-observed processes is essential for improved modelling, avoiding soil and water degradation, and minimising losses (Cerdan et al. 2002; Hessel and van Asch 2003; Jetten et al. 2003; Nearing et al. 2005; Starkloff and Stolte 2014; Pandey et al. 2016). Physically based models, such as LISEM, WEPP, ANSWERS, and SHETRAN, offer detailed descriptions of hydrological and erosive processes, but require numerous spatially distributed parameters related to soil and land use conditions (de Vente et al. 2013; Dymond and Vale 2018). These models explicitly incorporate properties such as hydraulic conductivity, antecedent moisture, texture, soil properties, and surface characteristics for each cell, using equations that describe infiltration, runoff, and erosion processes (Jetten et al. 2003; Le Bissonnais et al. 2005). Although soil detachment processes are similar across scales, re-infiltration, deposition, connectivity, terrain, riparian vegetation, and cropland characteristics introduce nonlinearities (Carson and Kirkby 1972). Thus, larger catchment areas do not necessarily yield proportionally greater sediment loads (Walling 1999; de Vente et al. 2007). Hillslope-scale studies are therefore essential for identifying runoff and erosion mechanisms that are often overlooked at broader scales and for improving model parameterization, particularly in no-till systems characterised by deep soils, with slopes ranging from 5% to 10%, and hillslope lengths often exceeding 1000 m (Bertol et al. 2000; Morais and Cogo 2001; Tondello Barbosa et al. 2021). However, the limited number of hillslope-scale monitoring studies and evaluation of model efficiency for representing runoff under no-till, make it difficult to incorporate this management system into hydrological and erosion models.

Model calibration is often based on limited hydrological data collected exclusively at the catchment outlet, which can introduce substantial uncertainties, particularly in large catchments where re-infiltration, deposition, and sediment delivery ratios vary widely. Additionally, sediment yield measured at outlet typically represents only a fraction of the total gross erosion that occurs across hillslopes (Minella et al. 2014; de Vente et al. 2007; Walling 1983). Proposing effective soil and water conservation practices for no-till crop systems requires accurate model parametrization that reflect different soil surface conditions at the hillslope scale.

Therefore, this study has two main objectives: (i) to model runoff and sediment yield on hillslopes representative of no-till agriculture in Southern Brazil using the LISEM model; and (ii) to evaluate the accuracy of LISEM-estimated infiltration by comparing it with field-measured apparent infiltration. These analyses aim to improve the understanding of hydrological and erosive processes under conservation agriculture and to support the development of more reliable modelling approaches for similar conditions.

2 | Materials and Methods

2.1 | Study Site

The monitoring units are located in a region representative of both soils and climate of the grain production system in southern Brazil (29°13′39″ S, 53°40′38″ W) (Figure 1). The climate is classified as Cfa (humid subtropical with no dry season and hot summers), characterized by well-distributed monthly rainfall (100–170 mm) (Alvares et al. 2013) and a mean daily reference evapotranspiration around 3–4 $mm.day^{-1}$ (Ferreira et al. 2019). Rainfall erosivity is considered very strong, around 10 657 $MJ.mm.ha^{-1}h^{-1}$ y^{-1}, based on records from 1976 to 2018 and calculated using the equation proposed by Ramon et al. (2017). The soils are highly weathered, deep, and contain more than 30% clay. They are classified as Rhodic Nitisol (Dystric) (IUSS Working Group WRB 2014), formed by extrusive

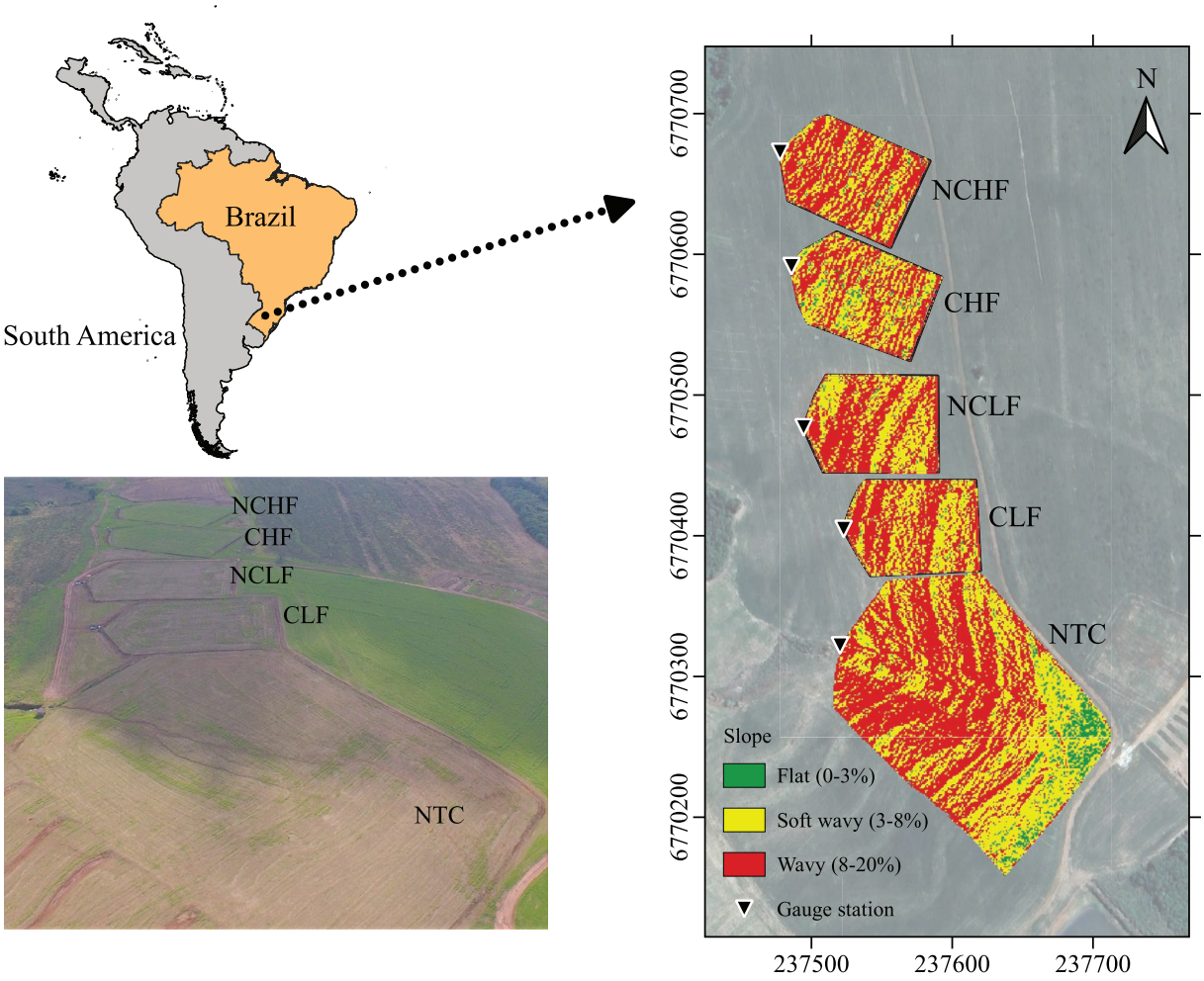

FIGURE 1 | Location of the study area in Southern America with the monitored units. Where: NTC is the no-till zero order catchment; CLF is the monitoring unit with chiselling and with low phytomass amount; NCLF is the monitoring unit without chiselling and with low phytomass amount; CHF is the monitoring unit with chiselling and with high phytomass amount; and, NCHF is the monitoring unit without chiselling and with high phytomass amount. "Phytomass" refers to plant biomass.

volcanic rocks (basalt), and are representative of those found across the Brazilian meridional plateau.

The monitoring units were paired and installed over a gentle hillslope with slopes ranging between 3% and 20%. Five units were monitored: four macroplots (~0.6 ha each) and one zero-order catchment (NTC, with an area of 2.4 ha) (Figure 1).

The NTC catchment measured 200 m in length and 135 m in width. Its topography is characterised by a negative plan curvature (convergent flow), forming a thalweg, and a negative profile curvature (convex). In contrast, the macroplots were ~100 m long and ~65 m wide, with zero plan curvature (no thalweg), and slightly negative profile curvature. The area where the monitoring units were installed was characterised by a topographical survey with a total station. This allowed for the optimal allocation of the units and the generation of a 1 × 1 m Numerical Elevation Model.

For each unit, soil physical properties (texture, saturated hydraulic conductivity, porosity, and bulk density) were analyzed at nine sampling points and three depths (5, 15, and 30 cm) to ensure homogeneity of the soil physical-hydric properties within each unit and among them (Londero, Minella, Schneider, et al. 2021; Deuschle et al. 2019).

2.2 | Soil and Crop Management

All units were cultivated under a no-till system; however three management factors varied among them and were expected to influence hydrological and erosion processes:

- Chiselling: with chiselling (C) or without chiselling (NC);
- Soil cover input: with low phytomass (LF) or high phytomass (HF) inputs;
- Scale: long-length slope with a thalweg (NTC) or short-length slope without a thalweg (CLF, NCLF, CHF, and NCHF).

The four macroplots combined various chiselling and soil cover inputs: (1) CLF, (2) NCLF, (3) CHF, and (4) NCHC. The zero-order catchment (NTC) corresponded to the macroplot (2) NCLF condition in terms of absence of chiselling and soil cover input, and was therefore used to evaluate scale effects (in terms of slope

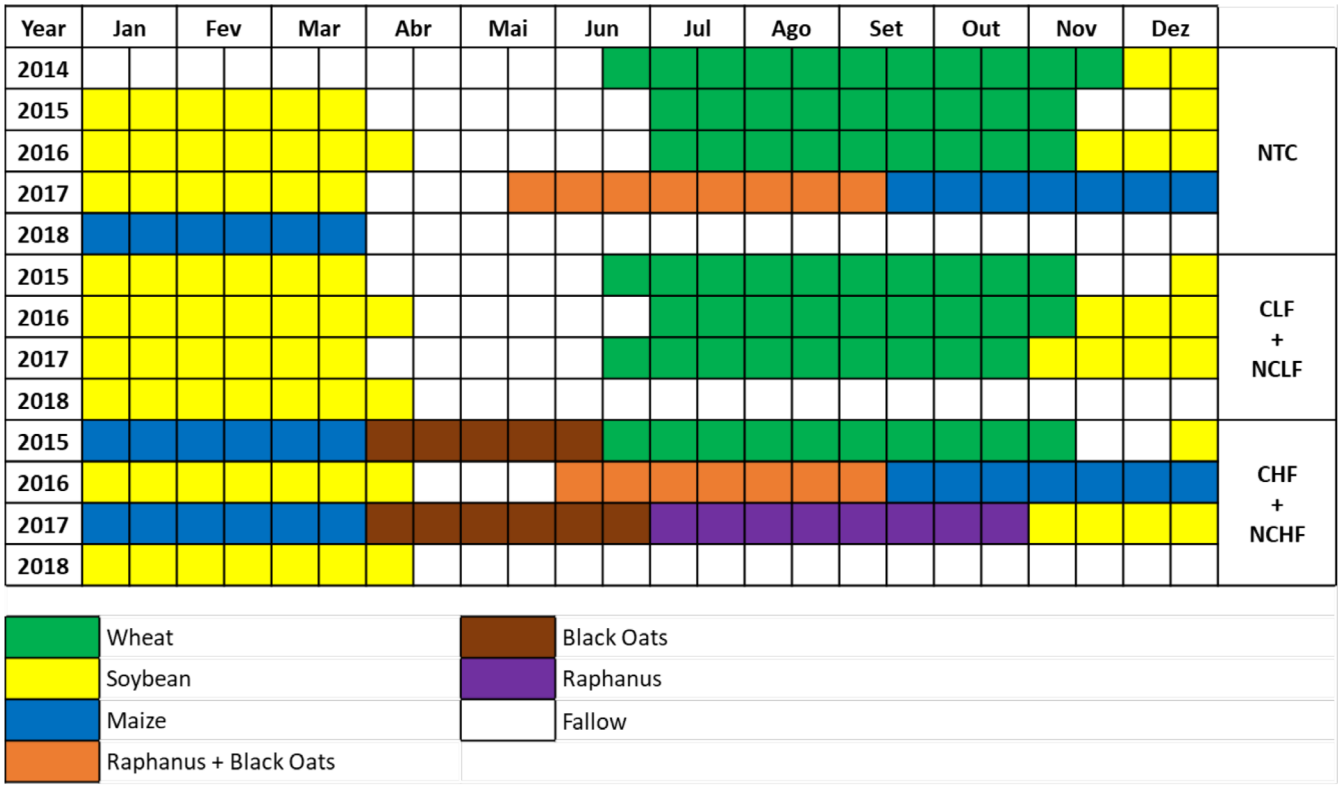

FIGURE 2 | Crop management throughout the monitored years. Where: NTC is the no-till zero-order catchment; CLF is the monitoring unit with chiselling and with low phytomass amount; NCLF is the monitoring unit without chiselling and with low phytomass amount; CHF is the monitoring unit with chiselling and with high phytomass amount; and, NCHF is the monitoring unit without chiselling and with high phytomass amount.

length and thalweg). The combination of these management factors has the potential to alter infiltration, re-infiltration, surface runoff generation and velocity, splash and flow detachment, and sediment deposition. Thus, the hydrological behaviour of each unit was analysed in the models to evaluate their respective sensitivity to these no-till configurations.

Chiselling was performed twice during the entire monitoring period: at the beginning of the experiment (2014) and again in 2016.

Crop management followed different crop rotations. The LF condition (~4 $t\,ha^{-1}\,year^{-1}$ of dry matter) reflects the most commonly used phytomass amount by local farmers, whereas the HF condition (~12 $t\,ha^{-1}\,year^{-1}$) represents phytomass amounts achieved under improved crop rotation without fallow periods. In the NTC catchment, the LF condition was used from 2014 to 2017, after which the system transitioned to HF (Figure 2).

All units received the same fertiliser applications, seeding, pesticide treatments, and harvesting operations, and were managed using the same equipment and field layout. This ensures that the surface roughness was not influenced by differences in agricultural operations.

2.3 | Hydrological Monitoring

The entire monitoring period included 61 rainfall-runoff events in the NTC catchment (July 2014 to April 2018) and 27 events in the macroplots (July 2015 to April 2018). For this study, 15 events from the NTC and 11 from the macroplots were selected (Table 1). Not all rainfall events were monitored in all units; thus, some events were monitored in both the NTC and macroplots, while others were recorded only in one scale. The selected events represent a range of rainfall magnitudes and seasonal conditions. Smaller magnitude events were not considered because they generated minimal runoff and sediment losses.

Rainfall measurements (mm and $mm.h^{-1}$) were obtained using daily manual rain gauges and an automatic rain gauge recording at 5-min intervals. Each monitoring unit was delineated with soil ridges to isolate its contributing area, and surface runoff was directed toward an H-type flume for measuring the streamflow rate and suspended sediment concentration.

At the H-type flumes (Figure 3), pressure transducers recorded continuous water level data during each rainfall event. Before their installation, water levels were measured manually every 10 min. From 2014 to 2016, only the NTC catchment had a pressure transducer, with readings every 2 min. In 2016, pressure transducers were installed in the macroplots, recording at 5-min intervals for all the monitoring units. Water depth was converted to surface runoff flow (q—$l.s^{-1}$) using specific rating curves for each H-type flume. The flume in the NTC was 0.6096 m wide and 0.4572 m wide in the macroplots. Manual water level measurements were taken at 10-min intervals or whenever notable changes occurred within the flume, using a staff gauge. These manual measurements were used as a reference to validate the automatic records, ensuring their accuracy and reliability. This

TABLE 1 | Antecedent 3-day and 24-h rainfall, total rainfall depth, mean rainfall intensity (I_{mean}), and maximum 30-min rainfall intensity (I_{30}) for all monitored events used in the calibration and validation of the LISEM model.

Date	3-day antecedent rainfall	24-h antecedent rainfall	Rainfall depth (mm)	I_{mean} (mm. h^{-1})	I_{30} (mm. h^{-1})	Monitoring unit	
						NTC	Macroplots
06/24/2015	52	17	52	5	8	X	
07/14/2015	29	29	19	3	19	X	X
07/20/2015	16	12	49	6	18		X
09/20/2015	85	69	20	3	19	X	
10/08/2015	36	35	160	8	58	X	X
11/19/2015	13	1	73	47	107	X	
12/14/2015	43	43	48	3	11	X	
12/23/2015	60	31	58	35	52	X	X
12/24/2015	133	103	84	8	26	X	X
12/29/2015	2	2	41	9	31	X	
10/17/2016	44	12	66	10	46	X	
10/18/2016	162	118	44	6	22	X	
05/26/2017	42	12	36	14	56		X
06/08/2017	6	0	98	5	21		X
10/11/2017	56	51	27	24	45		X
10/12/2017	99	72	22	13	26		X
01/21/2018	45	20	46	4	9	X	X
02/10/2018	20	20	92	59	91	X	X
02/20/2018	6	6	60	10	27	X	
03/15/2018	0	0	82	13	83	X	

Note: In the "Monitoring unit" columns, *X* indicates that the event was included in the LISEM simulations.

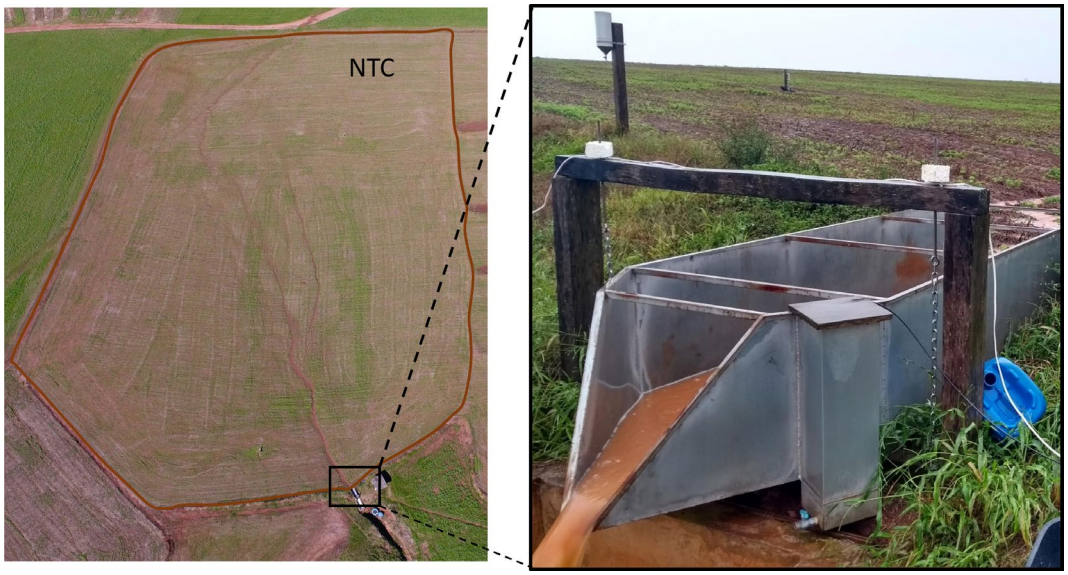

FIGURE 3 | Measurement techniques at the gauge station: NTC boundary and H-Type flume. Where: NTC is the no-till zero-order catchment.

cross-verification process allowed for the identification and correction of potential errors in data collection or interpretation, thereby improving the overall quality of the dataset.

High temporal resolution precipitation (P) and surface runoff flow (q) measurements (2–5 min intervals) were essential for describing runoff generation and propagation and for improving model parameterization. The resulting hydrographs and hyetographs, from the combination of high temporal resolution and in-field monitoring, were critical for interpreting hydrological responses and for accurate modeling at this scale.

Suspended sediment concentration (SSC—mg.l^{-1}) was analyzed from manually collected water samples throughout the monitoring period. Sampling occurred every 15–30 min or according to water level changes, ensuring adequate representation of both rising and falling limbs of the hydrograph.

Samples were analysed in the laboratory using the evaporation method (Shreve and Downs 2005). Results were linearly interpolated to obtain 1-min SSC records. Sediment yield (SY) was calculated using SSC of the samples collected during the rainfall event. Sediment discharge (SD—g.s^{-1}) was determined by multiplying SSC and q, with appropriate unit conversions.

2.4 | Hydrological Modelling

The no-till conditions of the five monitoring units were implemented in the Limburg Soil Erosion Model (LISEM) version 5.97, with a temporal resolution of 20 s and a spatial resolution of 5 m.

LISEM is a physically based, distributed erosion model that includes two modules, one for runoff and a second for erosion. The model requires spatially distributed input parameters that describe hydraulic and mechanical properties of the soil surface and information derived from relief. Accurate characterization of soil hydraulic properties for each unit was essential due to the uncertainties associated with model parameterization under different no-till configurations.

All inputs were provided in a spatially distributed form. The digital elevation model (DEM) was used to propagate the fluxes and to define hydrograph characteristics. More detailed information on LISEM's input parameters and equations used in the runoff and erosion modules is provided in Appendix 2.

2.4.1 | Runoff Module

The input variables for the runoff module included rainfall intensity (mm h^{-1}), surface cover, leaf area index, plant height, roughness (Manning's n and micro-depression), saturated hydraulic conductivity (K_{sat}), soil porosity, and initial soil moisture.

Vegetation related parameters were measured in different seasons, considering plant growth stages and events for each monitoring unit and modelled event. These included litter storage (amount of cover provided by crops, expressed in millimetres), vegetation height (vertical distance from the ground to the top of the vegetation canopy), fractional vegetation cover (proportion of the ground covered by vegetation), obtained from field visual observations, and leaf area index (LAI—total leaf area per unit ground area), which was obtained from the literature and used to determine the maximum canopy storage (Hamada and Pinto 2001; Romano 2005).

To determine micro-depression storage capacity, a pin-profilometer (with a length of 1 m and a 2 cm resolution) was used in two directions at six points in each macroplot and nine points in the NTC.

The Green and Ampt method was selected to simulate soil infiltration. Physical property parameters were obtained by analyzing undisturbed soil samples. K_{sat} and soil porosity were measured in the laboratory with three replicates at three depths (5, 15, 30 cm) at eight points in the NTC and six points in the macroplots.

Antecedent soil moisture content was determined by dividing the water retention curve into three categories: saturated soil (0–0.1 mca), field capacity (0.1–1 mca), and dry soil (>1 mca). For each modelled event, the 3-day antecedent rainfall (as listed in Table 1) was used to estimate the soil moisture deficit following the Curve Number (NRCS 2009) approach. Rainfall depth >60 mm indicated saturated soil; 20–60 mm indicated field capacity; and <20 mm indicated dry soil. Based on the calibrated initial soil moisture content, the soil water potential was then estimated.

Considering that infiltration simulation is crucial for determining the runoff magnitude, infiltration results generated by the LISEM during the calibration were compared with the directly measured apparent infiltration. This ensured that LISEM's infiltration estimates were consistent with the observed hillslope-scale infiltration. Apparent infiltration in the monitored units was studied by Koppe et al. (2022), following the method of Hawkins and Cundy (1987). This technique estimates apparent infiltration by subtracting runoff from rainfall, as shown in Equation (1).

$$I_a = R - Q \tag{1}$$

where I_a is apparent infiltration (mm or mm.h^{-1}); R is rainfall (mm or mm.h^{-1}); Q is runoff (mm or mm.h^{-1}).

In this study, apparent infiltration for each time interval of the selected rainfall events was calculated. Because this method evaluates the monitoring units as a whole, the resulting apparent infiltration is assumed to closely represent actual conditions, with minimal evapotranspiration losses during rainfall events. However, the method does not account for water retained in the vegetation canopy or crop residues, which can temporarily intercept a portion of the precipitation. Nevertheless, under high-magnitude rainfall events and high humidity, this fraction is minimal and considered negligible. Apparent infiltration was adjusted using Equation (2), where maximum infiltration rate (I_m) was determined as a function of precipitation (Rose 2004).

$$I_a(R) = I_m \times \left[1 - e^{-\frac{R}{I_m}}\right] \tag{2}$$

where I_a is apparent infiltration rate (mm.h^{-1}); R is rainfall intensity (mm.h^{-1}); I_m is maximum apparent infiltration (mm.h^{-1}).

The value of I_m was determined using all events monitored in each unit. With the defined I_m, I_a was calculated for each time interval, rainfall event, and monitoring unit.

Apparent infiltration was then compared with LISEM simulated infiltration to verify the model's ability to represent the water infiltration process using the Green and Ampt method.

The one-dimensional kinematic wave method (1D) was used to simulate flow propagation processes, based on the local drain direction (LDD) network. Surface runoff propagation along the hillslope was represented using Manning's equation, with Manning's n coefficient representing the surface conditions. Given the no-tillage adopted in the study area, crop residue was considered a key factor in determining this coefficient. For this purpose, we adopted Manning's n coefficient values proposed by Engman (1986), which were derived from USDA monitoring units. For phytomass amounts between 0.6 and 2.4 Mg.ha^{-1}, a Manning's n value of 0.07 was used, and 0.3 for phytomass greater than 2.4 Mg.ha^{-1} (Engman 1986).

2.4.2 | Erosion Module

The erosion module required information on soil aggregate stability, rainfall kinetic energy, characteristic particle diameters (D_{50} and D_{90}), and soil cohesion. Aggregate stability was measured following the water-drop method described by Moro (2010), in which the number of drops required to reduce a soil aggregate by half is recorded. In the study, aggregate stability was set at 200 drops. Particle size was determined using a laser particle size analyser, and the D_{50} and D_{90} corresponded to 50 and 110 μm, respectively.

Soil cohesion, which is related to soil detachment by overland flow, was measured in the field using a Torvane Shear Device under saturated conditions. Six points were analysed in each monitoring unit, with three replicates, yielding maximum, average, and minimum values of 67, 52, and 46 kPa, respectively. Random roughness values were adjusted according to the crop growth stage. Higher random roughness was measured during events shortly after sowing, whereas roughness decreased over time with mulch degradation, influenced by temperature and rainfall.

2.5 | Calibration and Validation

For the NTC catchment, 15 events were used for calibration, and 11 were used for the macroplots. Some events occurred in both monitoring units, while others were unique to either the NTC or the macroplots.

Calibration of rainfall events in LISEM was based on the model's ability to accurately represent surface runoff volume and to simulate the shape of the hydrograph and sediment discharge. The individually analysed variables were peak runoff, runoff volume, and sediment yield. Model performance was evaluated using Percent Bias (PBIAS), in which values between 15% and 25% are considered satisfactory for peak runoff and runoff volume, and values below 10% are considered excellent. For sediment yield, performance criteria are more flexible, with PBIAS values up to 55% considered satisfactory (Moriasi et al. 2015). Hydrograph and sediment discharge performance were evaluated using the Nash–Sutcliffe efficiency (NSE), where values below 0.5 are unsatisfactory, values between 0.5 and 0.65 are satisfactory, values between 0.65 and 0.75 are good, and values between 0.75 and 1 are very good (Moriasi et al. 2015).

To validate the model, we applied K-fold cross-validation, dividing the dataset into three groups according to I_{30}, ensuring that all rainfall events were used once during the validation step. Cross-validation improved validation robustness (Wong and Yang 2017; Arabameri et al. 2021). This approach systematically partitions and rotates events between calibration and validation sets and is particularly effective in scenarios where the number of rainfall events is limited. The rainfall events selected for the procedure are shown in the Tables 2 and 3 for the NTC and macroplots, respectively. For the validation runs, hydrological parameters were set to the median of the calibrated parameter values (K_{sat}, Manning's n coefficient, random roughness, and soil cohesion), while soil moisture was adjusted according to antecedent rainfall conditions.

The main parameters used for LISEM calibration were antecedent moisture, K_{sat}, Manning's n coefficient, random roughness, and soil cohesion. These parameters were selected because they play a critical role in the model's hydrological and erosion processes and exhibit high sensitivity, directly affecting simulated runoff, erosion, and sediment yield. All remaining parameters were kept as measured in the field made during each rainfall event. Given the high spatial and temporal variability of K_{sat}, this parameter was adjusted to improve runoff volume estimation, due to its direct influence on infiltration capacity. Manning's n coefficient, which directly affects flow velocity, was calibrated to better reproduce the hydrograph, particularly peak runoff. Manning's n also shows significant temporal variability due to changes in surface conditions, driven by variations in crop cover and residue levels over time.

3 | Results and Discussion

3.1 | Results of the Calibrated Events With the LISEM Model

The results for runoff peak (q_{peak}), runoff volume (Q), and sediment yield (SY), along with their respective PBIAS values, are presented in Table 4. Overall, nearly all results for the three variables were satisfactory, with most events having excellent performance.

For the NTC catchment, the calibration performance ranged from satisfactory to very good, based on commonly accepted statistical criteria. Among the 11 calibrated rainfall events, runoff volume was rated as good (PBIAS < ±15) for four events (06/24/2015, 09/20/2015, 01/21/2018, and 03/15/2018), and as very good (PBIAS < ±10) for the remaining ones, following Moriasi et al. (2007). For peak runoff, only two events showed

TABLE 2 | Rainfall events assigned to each K-fold calibration and validation step for the NTC monitoring unit.

Monitoring unit	K-fold	Simulation	Rainfall event	Rainfall depth (mm)	I_{30} (mm.h^{-1})
NTC	1	Calibration	07/14/2015	19	19
			09/20/2015	20	19
			10/08/2015	160	58
			11/19/2015	73	107
			12/14/2015	48	11
			12/23/2015	58	52
			12/24/2015	84	26
			12/29/2015	15	27
			01/21/2018	46	9
			02/20/2018	60	27
		Validation	06/24/2015	52	8
			03/15/2018	82	83
			02/10/2018	92	91
			10/17/2016	66	46
			10/18/2016	44	22
	2	Calibration	06/24/2015	52	8
			09/20/2015	20	19
			10/08/2015	160	58
			11/19/2015	73	107
			12/23/2015	58	52
			12/29/2015	15	27
			10/17/2016	66	46
			10/18/2016	44	22
			02/10/2018	92	91
			03/15/2018	82	83
		Validation	02/20/2018	60	27
			01/21/2018	46	9
			12/14/2015	48	11
			07/14/2015	19	19
			12/24/2015	84	26
	3	Calibration	06/24/2015	52	8
			07/14/2015	19	19
			12/14/2015	48	11
			12/24/2015	84	26
			10/17/2016	66	46
			10/18/2016	44	22
			01/21/2018	46	9
			02/10/2018	92	91
			02/20/2018	60	27
			03/15/2018	82	83

(Continues)

TABLE 2 | (Continued)

Monitoring unit	K-fold	Simulation	Rainfall event	Rainfall depth (mm)	I_{30} (mm.h^{-1})
NTC	3	Validation	11/19/2015	73	107
			09/20/2015	20	19
			12/29/2015	41	31
			12/23/2015	58	52
			10/08/2015	160	58

Note: Where: NTC = no-till zero order catchment.

PBIAS values above ±15%, which is within the satisfactory range (±15 to ±25), while the remaining events achieved very good performance (PBIAS < ±10). Overall, the hydrological calibration demonstrated robust and consistent performance across all rainfall events.

Six rainfall events with available sediment yield data were calibrated for the NTC. Among these, only the events of 07/14/2015 and 10/17/2016 presented PBIAS values above 15% (classified as good), whereas the remaining events achieved very good performance (PBIAS < ±15), based on the thresholds proposed by Moriasi et al. (2007). Although these two events showed higher PBIAS values, the soil loss differences were minimal, 4 kg for the 07/14/2015 event and 3 kg for the 10/17/2016 event, considering the 2.4 ha area of the NTC catchment. These results suggest that the model effectively captured sediment yield dynamics within the catchment.

This performance can be largely attributed to the physical and environmental characteristics of the NTC catchment, particularly the role of vegetative cover and no-till practices in reducing sediment and water losses. The low sediment yield and water loss observed during these events can be attributed to the dense vegetative cover, which reduces detachment by stabilizing the soil and intercepting rainfall energy. No-till provides protection against raindrop impact, preventing soil crust formation and minimizing soil loss (Almeida et al. 2021). The limited water loss also suggests that runoff lacked sufficient erosive energy (Wolschick et al. 2021).

NSE values for both hydrographs and sediment discharge in the NTC catchment indicated very good model performance (0.75–1), typically around 0.90, demonstrating strong agreement between observed and simulated data. However, the event of 10/17/2016 yielded an NSE of 0.76 (satisfactory), while the events on 10/18/2016 and 01/21/2018 showed unsatisfactory performance (NSE < 0.50). These deviations may be attributed to uncertainties in input data, model parameterization, or atypical rainfall–runoff dynamics during these specific events.

Figure 4 illustrates the simulation of two high-intensity rainfall events, for which the model satisfactorily represented runoff propagation and sediment discharge.

Sediment discharge in the NTC catchment showed a very good result only for the rainfall event of 12/23/2015. Lower soil disturbance and higher aggregation increased soil cohesion, making soil detachment more difficult to simulate. Nonetheless, sediment yield calibration showed excellent results for the NTC catchment.

Calibration for the CLF and NCLF macroplots also resulted in good performance for q_{peak}, runoff volume, and sediment yield.

The event of 10/08/2015 showed good performance (±15 < PBIAS < ±30) for all three variables. Its high rainfall intensity (maximum 30 min intensity (I_{30}) of 58 mm.h^{-1}) combined with the small size of the monitoring unit (~0.6 ha) contributed to a shorter concentration time. Manual water level and SSC measurements (every 10 to 15 min) may have introduced uncertainty and underestimated observed water level values due to low temporal resolution, meaning that the simulated values could potentially be closer to the actual hydrological response.

The event of 01/21/2018 was of low magnitude as initial rainfall increased soil moisture and runoff was generated only after saturation. Although LISEM provides multiple options for simulating infiltration, the Green-Ampt method was applied here. This method assumes Hortonian flow and uniform contribution to surface runoff over the entire area, particularly under saturated soil conditions (Bronstert et al. 2014). When the soil is not saturated, LISEM struggles to reproduce heterogeneous runoff patterns, due to the heterogeneity of saturated zones.

For the NCLF macroplot, only one event (01/21/2018) had a PBIAS > ±25 for q_{peak}, while runoff volume for the 07/14/2015 event was unsatisfactory (PBIAS > ±55). Sediment yield PBIAS remained < ±30 across the four analysed events for both CLF and NCLF. q_{peak} and runoff volume results were negatively affected by the 01/21/2018 and 07/14/2015 events, respectively. These poorer performances can be attributed to the units' small size and their distinct responses to rainfall events (De Roo and Jetten 1999). LISEM may not have accurately captured these processes. In a study conducted in southern Brazil, LISEM calibration performed well for runoff and sediment yield in small catchments; however, some parameters, such as saturated hydraulic conductivity (K_{sat}), initial soil moisture, and erosion-related parameters, required adjustments. Validation showed weaker agreement between the simulated and observed values, emphasising the need for long-term hydrosedimentological monitoring and detailed characterisation of soil parameters, which could be crucial for improving validation results (Ebling et al. 2024).

The units were bordered by embankments to prevent external water inflow. At the base of the plot, runoff was directed toward the H-flume, but the embankment system can introduce delays, especially in the units of linear shape, meaning that

TABLE 3 | Rainfall events assigned to each K-fold calibration and validation step for the macroplots.

Monitoring unit	K-fold	Simulation	Rainfall event	Rainfall depth (mm)	I_{30} (mm.h^{-1})
Macroplots	1	Calibration	07/20/2015	49	18
			10/08/2015	160	58
			12/24/2015	84	26
			05/26/2017	36	56
			06/08/2017	98	21
			10/12/2017	22	26
			02/10/2018	92	91
		Validation	01/21/2018	46	9
			10/11/2017	27	45
			07/14/2015	19	19
			12/23/2015	58	52
	2	Calibration	07/14/2015	19	19
			07/20/2015	49	18
			12/23/2015	58	52
			10/11/2017	27	45
			10/12/2017	22	26
			01/21/2018	46	9
			02/10/2018	92	91
		Validation	05/26/2017	36	56
			06/08/2017	98	21
			10/08/2015	160	58
			12/24/2015	84	26
	3	Calibration	07/14/2015	19	19
			10/08/2015	160	58
			12/23/2015	58	52
			12/24/2015	84	26
			05/26/2017	36	56
			06/08/2017	98	21
			10/11/2017	27	45
			01/21/2018	46	9
		Validation	02/10/2018	92	91
			10/12/2017	22	26
			07/20/2015	49	18

the runoff first reaches the embankment before being directed to the flume. In contrast, in the NTC catchment, runoff naturally converges toward the thalweg, where the H-flume is located, improving model performance at this scale. Accurate representation of flow pathways depends on the DEM and the LDD, which determine runoff propagation (Dávila-Hernández et al. 2022).

Hydrograh modeling for CLF and NCLF showed similar difficulties. The 07/14/2015 event exhibited delays possibly due to inconsistencies in manually collected data. The 01/21/2018 event was complex because runoff was not generated initially, and only occurred later, resulting in a PBIAS > ±25. Sediment discharge in the CFL macroplot is difficult to compare with NCLF, partly due to differences in *SSC* sampling frequency. Manual sampling

TABLE 4 | PBIAS statistics for runoff peak (q_{peak}), runoff volume (Q), and sediment yield (SY) for each calibrated rainfall event.

Monitoring unit	Event	q_{peako} ($L\,s^{-1}$)	q_{peaks} ($L\,s^{-1}$)	Q_o (m^3)	Q_s (m^3)	SY_o (kg)	SY_s (kg)	PBIAS (%)		
								q_{peak}	Q	SY
NTC	06/24/2015	18	18	321	357	NA	NA	−3.4	11.1	NA
	07/14/2015	13	16	50	45	22	26	23.4	−8.3	21.3
	09/20/2015	6	6	18	15	NA	NA	2.6	−15.7	NA
	10/08/2015	354	370	1723	1722	79	74	4.7	0	−6.9
	11/19/2015	457	472	905	822	NA	NA	3.2	−9.2	NA
	12/14/2015	29	30	203	199	NA	NA	4.4	−2.3	NA
	12/23/2015	283	290	1205	1102	448	428	2.5	−8.5	−4.5
	12/24/2015	138	141	1023	1007	108	109	2.1	−1.6	0.7
	12/29/2015	51	50	74	77	NA	NA	−0.5	3.5	NA
	10/17/2016	19	22	41	39	14	11	21.4	−6	−19.1
	10/18/2016	22	22	119	131	2	3	2.7	9.6	14.2
	01/21/2018	198	189	330	380	182	174	−5	15.1	−4.7
	02/10/2018	360	357	766	761	NA	NA	−1	−0.7	NA
	02/20/2018	49	44	115	130	NA	NA	−9.7	13.2	NA
	03/15/2018	18	18	321	357	NA	NA	−3.4	11.1	NA
CLF	07/14/2015	3	3	8	6	11	11	6.1	−16.8	−6.4
	07/20/2015	10	10	47	47	19	16	−8.7	−0.2	−16.8
	10/08/2015	92	110	318	399	25	20	19.5	25.2	−18.6
	12/23/2015	70	67	284	265	103	103	−4.1	−6.6	0.6
	12/24/2015	48	38	287	313	69	67	−21.2	9	−3.2
	05/26/2017	29	29	49	49	NA	NA	2.1	−0.1	NA
	06/08/2017	6	6	43	42	NA	NA	2.9	−1.8	NA
	10/11/2017	27	26	35	37	NA	NA	−4.9	6.7	NA
	10/12/2017	18	18	39	40	NA	NA	−3.4	2.5	NA
	01/21/2018	11	5	25	16	NA	NA	−53.5	37.6	NA
	02/10/2018	88	87	122	119	NA	NA	−0.8	−2.8	NA
NCLF	07/14/2015	3	3	8	6	26	24	7.4	−26	−8.5
	07/20/2015	11	12	60	63	41	36	2.3	4.7	−12.4
	10/08/2015	92	104	386	369	48	37	12.5	−4.3	−23.4
	12/23/2015	70	77	307	285	158	151	9.1	−6.9	−4.8
	12/24/2015	52	38	307	313	129	136	−27.5	1.8	5.5
	05/26/2017	70	68	92	98	NA	NA	−2.9	5.7	NA
	06/08/2017	9	9	80	67	NA	NA	0.7	−16.3	NA
	10/11/2017	38	39	49	48	NA	NA	3.4	−1.9	NA
	10/12/2017	26	27	49	45	NA	NA	4.5	−9.7	NA
	01/21/2018	20	5	40	16	NA	NA	−73.1	−59.8	NA
	02/10/2018	150	139	184	194	NA	NA	−6.9	5.6	NA

(Continues)

TABLE 4 | (Continued)

Monitoring unit	Event	q_{peako} ($L\,s^{-1}$)	q_{peaks} ($L\,s^{-1}$)	Q_o (m^3)	Q_s (m^3)	SY_o (kg)	SY_s (kg)	PBIAS (%)		
								q_{peak}	Q	SY
CHF	07/14/2015	2	2	6	3	1	1	22.5	−48.7	−9.2
	07/20/2015	6	6	34	23	5	5	8.4	−32.3	−3.9
	10/08/2015	81	108	329	334	12	8	33.9	1.5	−32.6
	12/23/2015	61	74	271	265	90	87	22.4	−2.5	−4.1
	12/24/2015	37	34	235	235	54	55	−6.9	0	1.5
	05/26/2017	46	45	82	71	NA	NA	−3.2	−13.6	NA
	06/08/2017	3	4	37	31	NA	NA	11.4	−16	NA
	10/11/2017	21	21	35	33	NA	NA	2.6	−4.1	NA
	10/12/2017	17	19	38	38	NA	NA	10.1	0.3	NA
	01/21/2018	3	3	7	8	NA	NA	1.3	14.8	NA
	02/10/2018	57	57	80	82	NA	NA	−0.4	2.4	NA
NCHF	07/14/2015	2	3	6	4	0	0	53.8	−39.2	22
	07/20/2015	7	7	39	32	3	1	−1.9	−17.2	−5.2
	10/08/2015	86	122	364	341	13	8	41.2	−6.4	−36.2
	12/23/2015	65	74	275	263	32	35	14	−4.5	8.5
	12/24/2015	33	32	207	224	21	21	−4.9	8.3	−3.9
	05/26/2017	94	94	132	123	NA	NA	0.8	−6.4	NA
	06/08/2017	6	6	63	58	NA	NA	5.7	−7.8	NA
	10/11/2017	41	43	59	58	NA	NA	5.1	−2	NA
	10/12/2017	25	24	51	70	NA	NA	−3.9	36.8	NA
	01/21/2018	2	2	4	4	NA	NA	10.2	10.8	NA
	02/10/2018	89	90	104	113	NA	NA	1.3	8.6	NA

Note: Where: q_{peako} = observed runoff peak; q_{peaks} = simulated runoff peak; Q_o = observed runoff volume; Q_s = simulated runoff volume; SY_o = observed sediment yield; SY_s = simulated sediment yield; NA = no data available. Monitoring units: NTC = no-till zero order catchment; CLF = chiselling with low phytomass amount; NCLF = no chiselling and low phytomass amount; CHF = chiselling and high phytomass amount; NCHF = no chiselling and high phytomass amount.

limited the temporal representation of *SSC*. Although automatic samplers could improve *SSC* resolution, they may face issues with suction in small-scale runoff collection, risking sediment overestimation; however they are useful for water quality studies determining nutrient concentrations (Wilson et al. 2024).

For the CHF and NCHF macroplots, calibration resulted in lower runoff peak and volume for the 01/21/2018 and 07/14/2015 events. The event of 10/08/2015 showed good performance for runoff volume (±10 < PBIAS < ±55), despite the runoff peak being overestimated. Sediment yield for the same event was underestimated due to the low frequency of *SSC* sampling, which was also observed in the low phytomass macroplots (CLF and NCLF). Hydrographs for the 07/14/2015 and 01/21/2018 events were difficult to model because of delayed and initially absent runoff. For sediment discharge, only the 12/23/2015 event achieved good performance in CHF and NCHF (±15 < PBIAS < ±30), due to more frequent *SSC* sampling.

Overall, calibration showed good performance (PBIAS < ±30) for the NTC catchment. For the macroplots, however, the model faced difficulties representing hydrological and erosive processes. Although LISEM was not designed for small plots (De Roo and Jetten 1999), it performs well at the hillslope scale, which is encouraging for catchment scale modelling. Accurate simulation at the hillslope scale suggests reliable performance at larger scales, although caution is needed regarding rainfall magnitude (de Vente et al. 2007). LISEM performs better under high-intensity and high-volume rainfall, when surface conditions are less significant. During such events, vegetation and soil management become less effective in controlling surface runoff (Deuschle et al. 2019; Londero, Minella, Schneider, et al. 2021; Fuentes-Guevara et al. 2024), and relief becomes the dominant factor (Liu et al. 2019). Parameters such as K_{sat}, Manning's n, and phytomass amount strongly influence the model, especially in a no-till system with deep soils, such as this study. However, no significant reduction in runoff was observed with increasing phytomass.

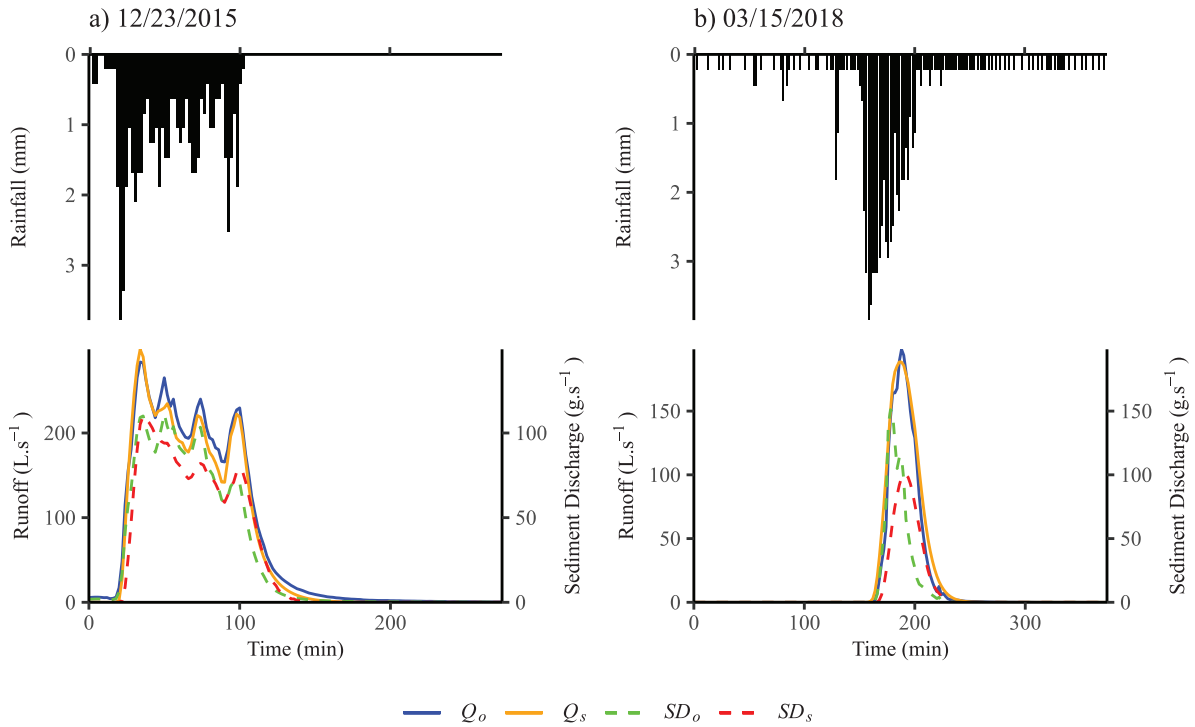

FIGURE 4 | Observed and simulated hydrographs and sediment discharge for the rainfall events of 12/23/2015 (a) and 03/15/2018 (b) in the NTC catchment. Where: Q_o is the observed runoff volume; Q_s is the simulated runoff volume; SY_o is the observed sediment yield; SY_s is the simulated sediment yield.

Phytomass plays a key role in enhancing aggregate stability, infiltration, productivity while reducing soil loss (Merten et al. 2015). These benefits, however, diminish during high-intensity rainfall or under high soil moisture antecedent conditions (Deuschle et al. 2019; Londero, Minella, Schneider, et al. 2021, 2021), when rainfall intensity becomes the controlling factor. In LISEM, vegetation interception is represented by parameters such as canopy openness, litter storage, LAI, cover height, and cover surface (Appendix 2).

LISEM showed good calibration performance for short-duration, high-intensity events at both studied scales, the NTC with convergent topography and the four macroplots with linear/planar curvature. The comparison between observed and calibrated peak runoff, runoff volume, and sediment yield produced NSE values >0.98, confirming very good calibration quality, as shown in Figure 5.

3.2 | Hydrological Component Calibration

Table 5 presents the average measured and calibrated values of K_{sat}, initial moisture content (θ_i), surface roughness (*RR*), and n for each monitoring unit. The calibrated K_{sat} values were lower than the measured ones in the macroplots (74% for CLF, 66% for NCLF, 54% for CHF, and 82% for NCHF), with the exception being the NTC, where the calibrated average was 57% higher than the measured value. In general, the K_{sat} calibration tends to result in lower values than field measurements (de Barros, Minella, Dalbianco, and Ramon 2014).

Estimated and calibrated θ_i values did not differ, as the selected calibration events occurred under high antecedent moisture. High moisture improves both simulation and calibration performance because LISEM simulates infiltration using a Hortonian process (Koppe et al. 2022). Under wetter conditions, the model is therefore more effective at simulating surface runoff.

Manning's *n* coefficient reflects the effect of surface residues in no-till systems. In LISEM, Manning's *n* is treated as constant during each rainfall-runoff simulation; however, it is known that this coefficient varies with soil surface conditions and flow depth (Julien 2018). Therefore, a specific Manning's *n* value was calibrated for each rainfall-runoff event. Manning's coefficient values used for this work were obtained from studies and experiments conducted under controlled conditions, either with simulated rainfall or water flow generating uniform runoff (Engman 1986; Julien 2018). Lower Manning's coefficient values are found in plots with lower amounts of residue, while larger residue amounts require higher *n* values to account for increased surface friction. The final calibrated values remain within the range observed in previous studies by Engman (1986), Te Chow et al. (1988), and Julien (2018).

RR had to be increased during calibration to delay the onset of runoff. This was likely due to the model generating runoff earlier than observed, due to its representation of the Hortonian process. Increasing *RR* helps delay runoff onset. *RR* can vary with management practices, particularly before and after sowing and harvesting. Depending on the volume and intensity of rainfall, soil type, and the distribution of soil aggregates, *RR* can decrease from sowing to harvest (Dalla Rosa et al. 2012).

Figure 6 shows the calibrated distributions of K_{sat}, n, RR, coh, and coh_{veg} for each K-fold. These parameters were adjusted to obtain satisfactory NSE and PBIAS values for peak runoff and runoff volume.

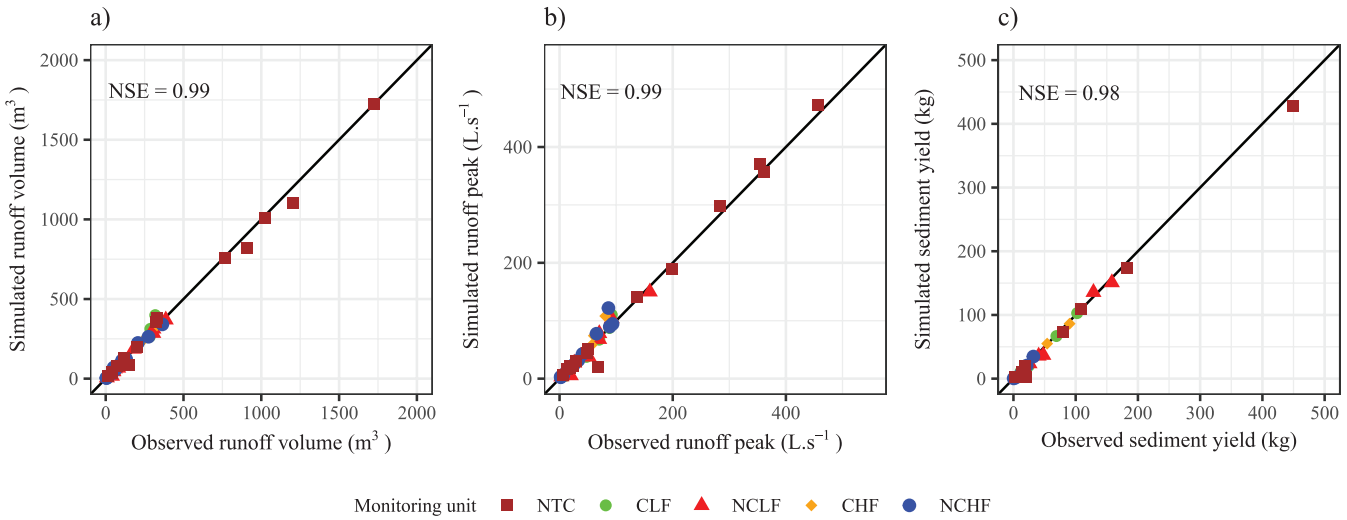

FIGURE 5 | Linear model of observed and calibrated (a) runoff volume, (b) runoff peak and (c) sediment yield from the LISEM model. Where: the continuous line represents the plane 1:1; NTC is the no-till zero order catchment; CLF is the monitoring unit with chiselling and with low phytomass amount; NCLF is the monitoring unit without chiselling and with low phytomass amount; CHF is the monitoring unit with chiselling and with high phytomass amount; and, NCHF is the monitoring unit without chiselling and with high phytomass amount.

TABLE 5 | Average calibrated and measured values of *K*sat, θ_i, RR, and Manning's *n* for each monitoring unit.

	NTC (*n* = 11)	CLF (*n* = 8)	NCLF (*n* = 8)	CHF (*n* = 8)	NCHF (*n* = 8)
			K_{sat} (mm. h^{-1})		
Calibrated	12.5	9.4	7.3	12.3	8.5
Measured	7.1	35.6	21.1	26.4	47.5
			θ_i (cm^3. cm^{-3})		
Calibrated	0.4	0.38	0.38	0.38	0.38
Estimated	0.39	0.38	0.38	0.38	0.38
			n (s.m $^{-1/3}$)		
Calibrated	0.27	0.21	0.17	0.20	0.18
Estimated	0.07	0.07	0.07	0.3	0.3
			RR (cm)		
Calibrated	1.6	1.4	1.7	1.5	2.0
Measured	1.1	1.1	1.1	1.1	1.1

Note: Where monitoring units: NTC = no-till zero order catchment; CLF = chiselling with low phytomass amount; NCLF = no chiselling and low phytomass amount; CHF = chiselling and high phytomass amount; NCHF = no chiselling and high phytomass amount.

The infiltration performance of LISEM after calibration was highly satisfactory when compared with apparent infiltration (I_a). The results of the calibration showed an improved accuracy and the calibrated parameters remained within the range of observed or determined data. As reported in previous studies (De Roo and Jetten 1999; Jetten et al. 2003; de Barros, Minella, Dalbianco, and Ramon 2014), K_{sat} often must be reduced substantially to achieve accurate simulations—a pattern also observed here for the macroplots—although the values remained within the range of observed variations. Other studies required adjustments to antecedent moisture and matrix potential due to the sensitivity of the Green-Ampt method to these parameters (De Roo and Jetten 1999; de Barros, Minella, Dalbianco, and Ramon 2014) (Appendix 1).

Manning's *n* commonly requires adjustment in LISEM applications (de Barros, Minella, Dalbianco, and Ramon 2014), being increased compared with the values reported in the literature (Hessel et al. 2006). In this study, Manning's n values remained consistent with the assumptions used for determining friction coefficients; they were not excessively high, whereas sometimes they exceed 1 (Julien 2018). RR was also adjusted to better represent the delay in runoff onset. Event-by-event comparisons generally indicated that, following calibration, LISEM accurately reproduced infiltration processes across different no-till hillslopes.

Figure 7 presents a comparison between LISEM's infiltration based on the Green-Ampt method versus infiltration derived by apparent infiltration. Infiltration was better represented for the NTC, compared with the macroplots, supporting the hypothesis that Green–Ampt and apparent infiltration methods perform more effectively at larger spatial scales, where small-scale variability is averaged out (Dunne et al. 1991; Yu et al. 2000). Dunne et al. (1991) also noted that apparent infiltration stabilizes at hillslope lengths greater than 100 m, a condition that more closely matches the NTC, rather than the macroplots.

Soil water infiltration is influenced by a combination of soil physical properties (e.g., texture, structure, and porosity), surface conditions (e.g., micro-roughness and residue cover), and hydraulic characteristics (e.g., K_{sat}). Although physically based models seek to incorporate these factors, the inherently dynamic nature of infiltration, affected by rainfall intensity, antecedent moisture, and soil surface sealing, makes accurate

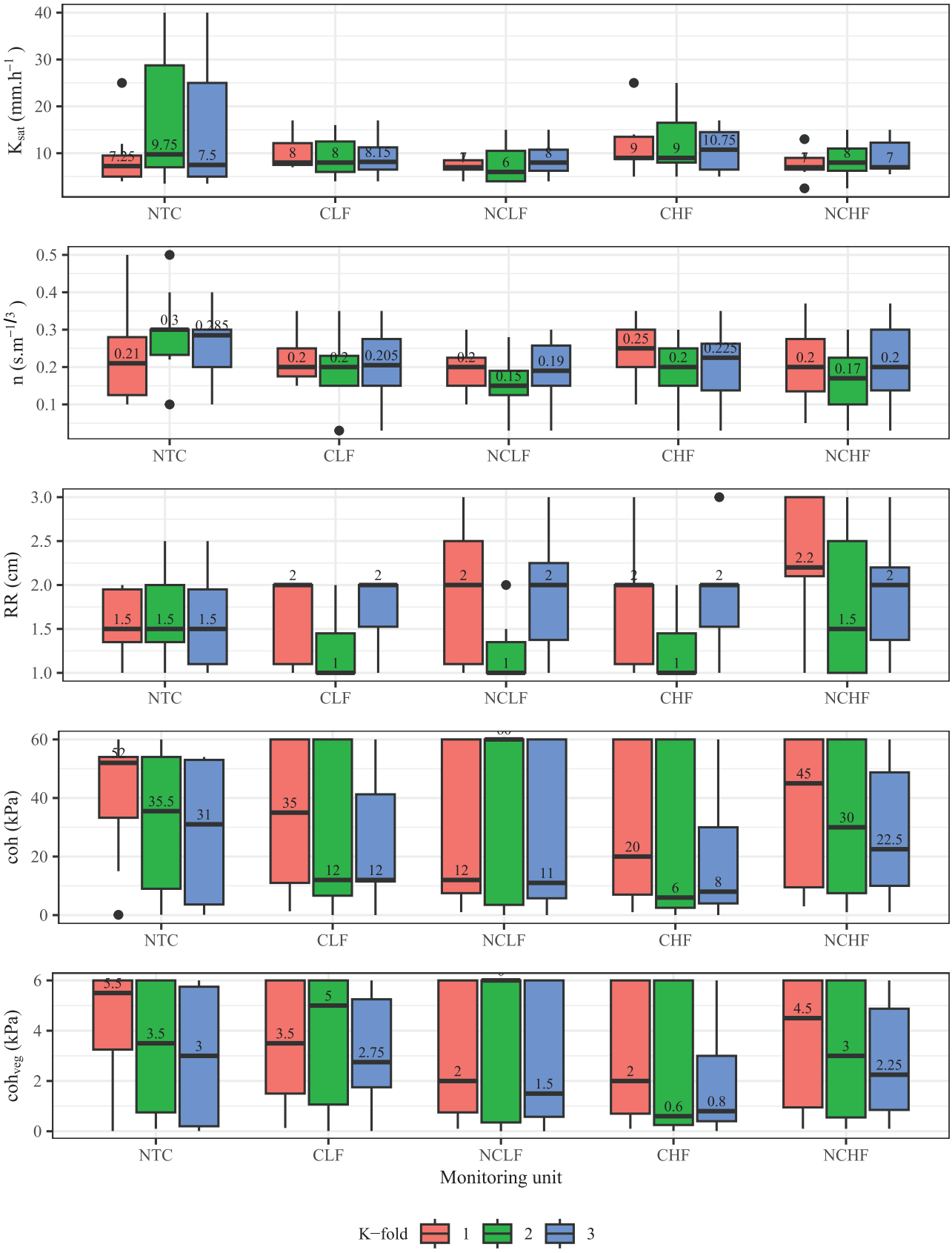

FIGURE 6 | Boxplots of saturated soil conductivity (K_{sat}), Manning's n coefficient (n), random roughness (RR), soil cohesion (coh), and additional soil cohesion by vegetation (coh$_{veg}$) for each monitoring unit and K-fold used during calibration. Where: NTC is the no-till zero order catchment; CLF is the monitoring unit with chiselling and with low phytomass amount; NCLF is the monitoring unit without chiselling and with low phytomass amount; CHF is the monitoring unit with chiselling and with high phytomass amount; NCHF is the monitoring unit without chiselling and with high phytomass amount; and the 1, 2, 3 represent the K-folds.

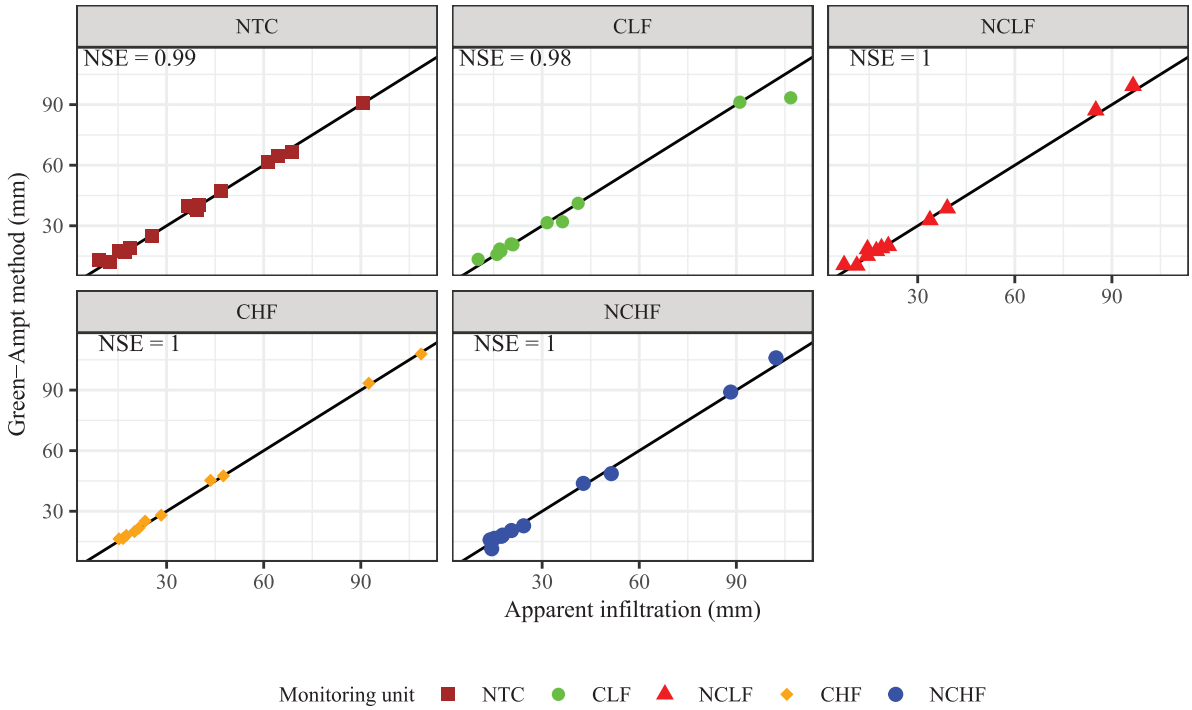

FIGURE 7 | Linear models comparing LISEM infiltration (Green-Ampt method) with apparent infiltration for each monitoring unit. Where: the continuous line represents the plane 1:1; NTC is the no-till zero order catchment; CLF is the monitoring unit with chiselling and with low phytomass amount; NCLF is the monitoring unit without chiselling and with low phytomass amount; CHF is the monitoring unit with chiselling and with high phytomass amount; and, NCHF is the monitoring unit without chiselling and with high phytomass amount.

TABLE 6 | Average and standard deviation (SD) of calibrated soil cohesion (coh) and cohesion of vegetation (coh_{veg}) parameters for each monitoring unit.

	NTC	CLF	NCLF	CHF	NCHF
			Coh (kPa)		
Average	19.37	12.08	4.25	4.25	12.25
SD	20.57	14.03	4.02	4.02	11.56
			Coh_{veg} (kPa)		
Average	2.02	2.16	0.43	0.43	1.18
SD	2.24	2.16	0.40	0.40	1.20

Note: Where monitoring units: NTC = no-till zero order catchment; CLF = chiselling with low phytomass amount; NCLF = no chiselling and low phytomass amount; CHF = chiselling and high phytomass amount; NCHF = no chiselling and high phytomass amount.

representation challenging. This is critical at smaller monitoring scales, such as the macroplots, due to their high spatial variability (Dunne et al. 1991; Yu et al. 2000). Small differences in roughness or porosity can cause significant deviations between simulated and observed infiltration.

In contrast, apparent infiltration integrates these factors over larger areas, reducing micro-scale noise and providing more stable and representative infiltration estimates at the plot or catchment scale. This reinforces its suitability for model evaluation, particularly when assessing average hydrological behavior in heterogeneous agricultural landscapes (Koppe et al. 2022).

Manning's n was adjusted within literature-reported limits (Engman 1986) until the simulated hydrograph aligned with observations, ensuring consistency with established flow dynamics. High Manning's n values are commonly used in LISEM (De Roo and Jetten 1999), especially shortly after sowing when roughness is greatest. Higher roughness increases runoff delay and peak time. Manning's n also controls recession times, as lower values yield faster recessions.

After calibration, RR values were similar across monitoring units, especially those with the same soil management. However, the chiselled units (CLF and CHF) had lower average *RR* than the non-chiselled ones (NTC, NCLF, and NCHF). Mean Manning's n was also similar among monitoring units, although higher values were observed for the NTC, followed by the chiselled plots (CLF and CHF), and lower values in the non-chiselled ones (NCHF and NCLF). This is consistent with the theory of friction parameters, in which higher residue cover and micro-roughness result in increased Manning's n values (Cogo et al. 1983, 2003; Engman 1986; Julien 2018).

3.3 | Erosive Component Calibration

The values of D_{50}, D_{90}, and soil aggregate stability were not adjusted across events and monitoring units, as they exhibited low sensitivity within the model. In contrast, soil cohesion and the additional cohesion due to the presence of roots were calibrated.

Table 6 presents the average measured and calibrated values of soil and vegetation cohesion for each monitoring unit. Soil cohesion

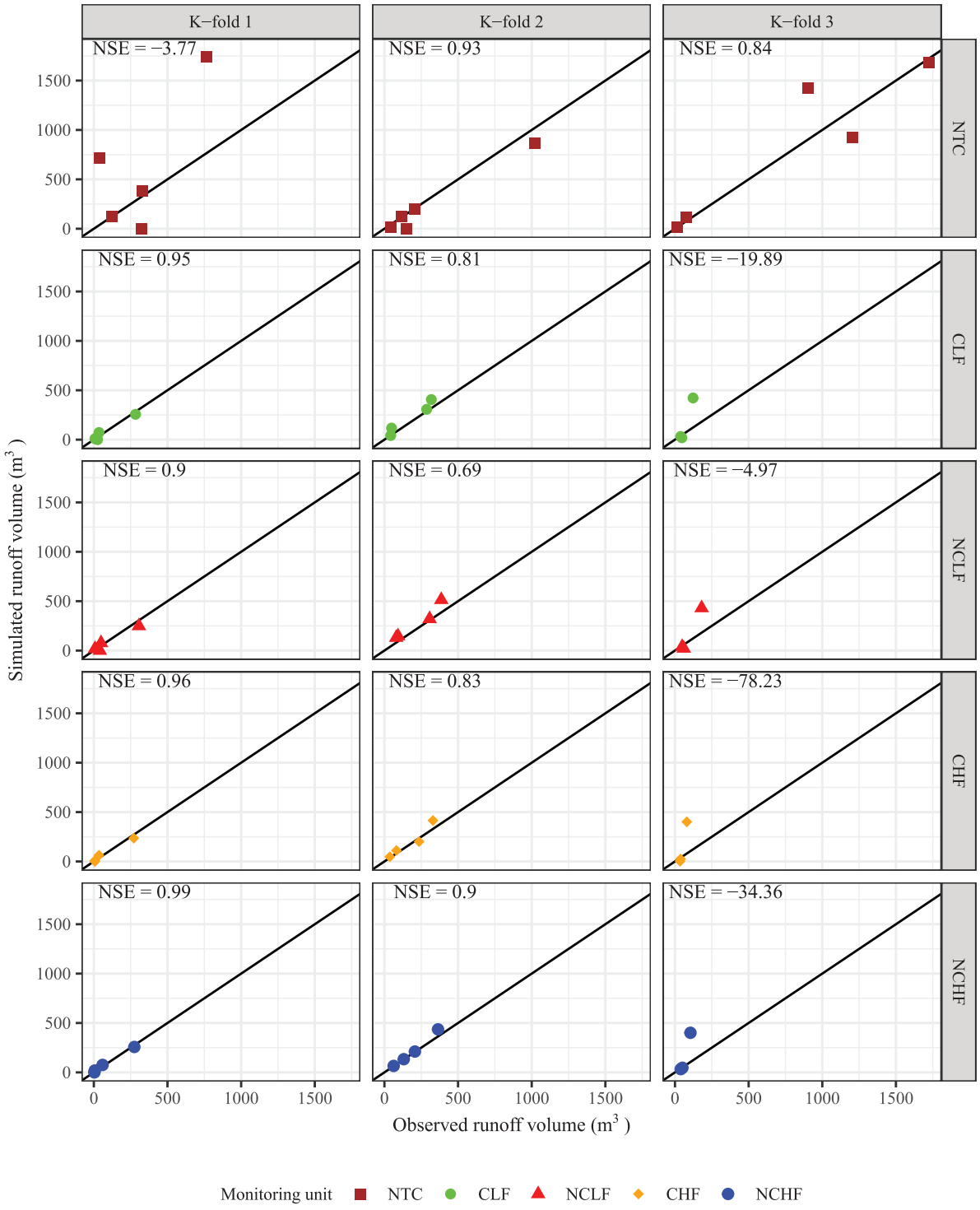

FIGURE 8 | Observed and simulated runoff volumes during the validation step for each K-fold and monitoring unit. Where: the continuous line represents the plane 1:1, NTC is the no-till zero order catchment; CLF is the monitoring unit with chiselling and with low phytomass amount; NCLF is the monitoring unit without chiselling and with low phytomass amount; CHF is the monitoring unit with chiselling and with high phytomass amount; and, NCHF is the monitoring unit without chiselling and with high phytomass amount.

values ranged from 4.25 to 19.37 kPa, with the highest average value observed in the NTC and the lowest in NCLF. Vegetation cohesion refers to the resistance of plants to be pulled out of the soil due to root strength; higher values suggest the vegetation is more effective in protecting the soil against erosion (Baets et al. 2008). Vegetation cohesion ranged from 0.43 to 2.16 kPa, with the highest average in CLF and the lowest in NCLF.

The variation in cohesion parameters did not follow a consistent or physically justified pattern, as multiple adjustments were required during calibration. In many cases, final calibrated values differed considerably from field or laboratory measured values. LISEM calibration highlighted soil cohesion as the parameter requiring the most substantial modifications to accurately reproduce sediment yield, which was initially overestimated,

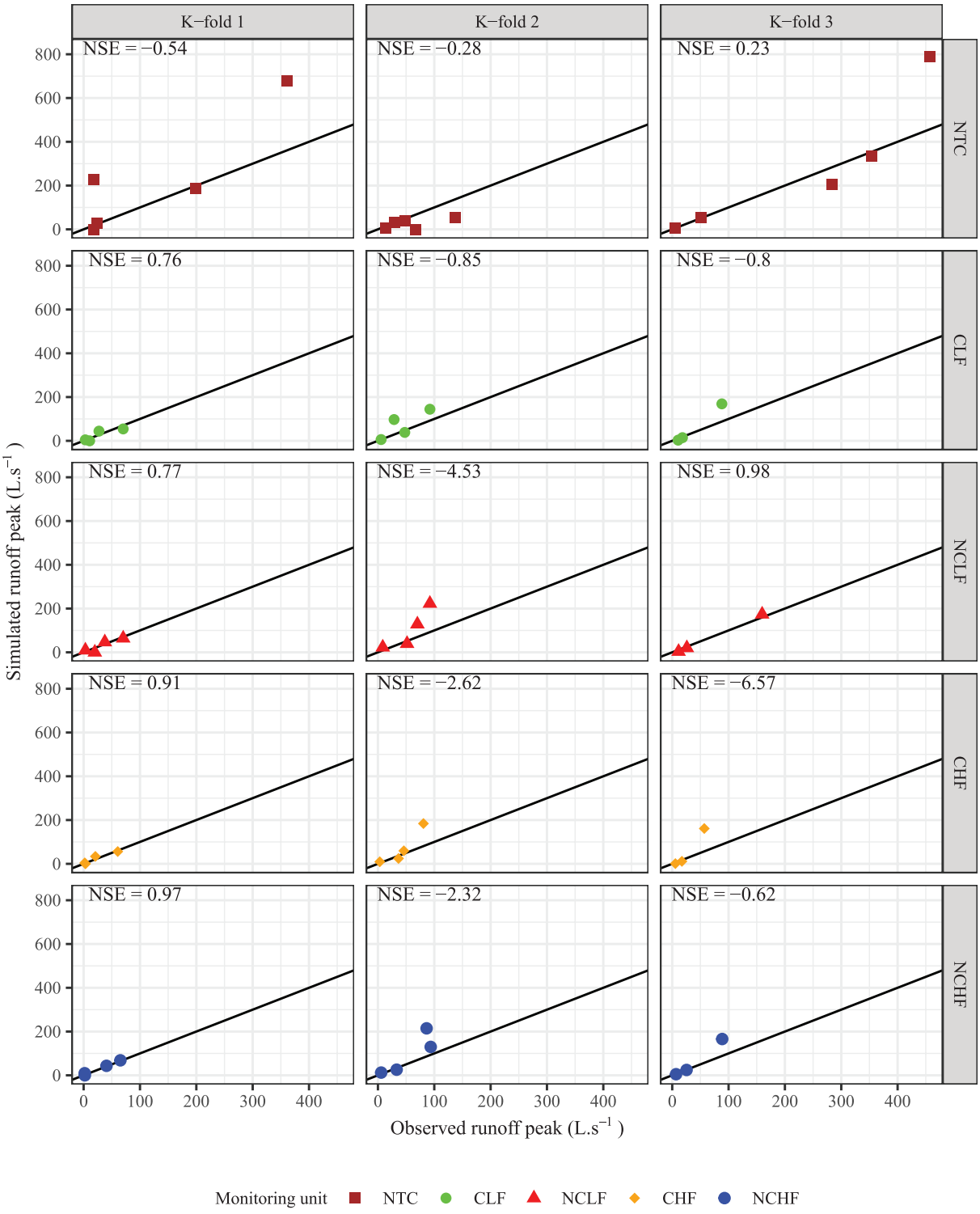

FIGURE 9 | Observed and simulated runoff peak during the validation step for each K-fold and monitoring unit. Where: the continuous line represents the plane 1:1, NTC is the no-till zero order catchment; CLF is the monitoring unit with chiselling and low phytomass amount; NCLF is the monitoring unit without chiselling and low phytomass amount; CHF is the monitoring unit with chiselling and high phytomass amount; and, NCHF is the monitoring unit without chiselling and high phytomass amount.

and consistent with results from de Barros, Minella, Dalbianco, and Ramon (2014) and Kværnø and Stolte (2012). While newer model versions, offering additional sediment yield calculation options, have shown improved performance in poorly weathered soil conditions (Schlesner 2017), the highly weathered and cohesive soils in this study demanded large reductions in soil cohesion to achieve results similar to those obtained for less cohesive soils (Hessel et al. 2006).

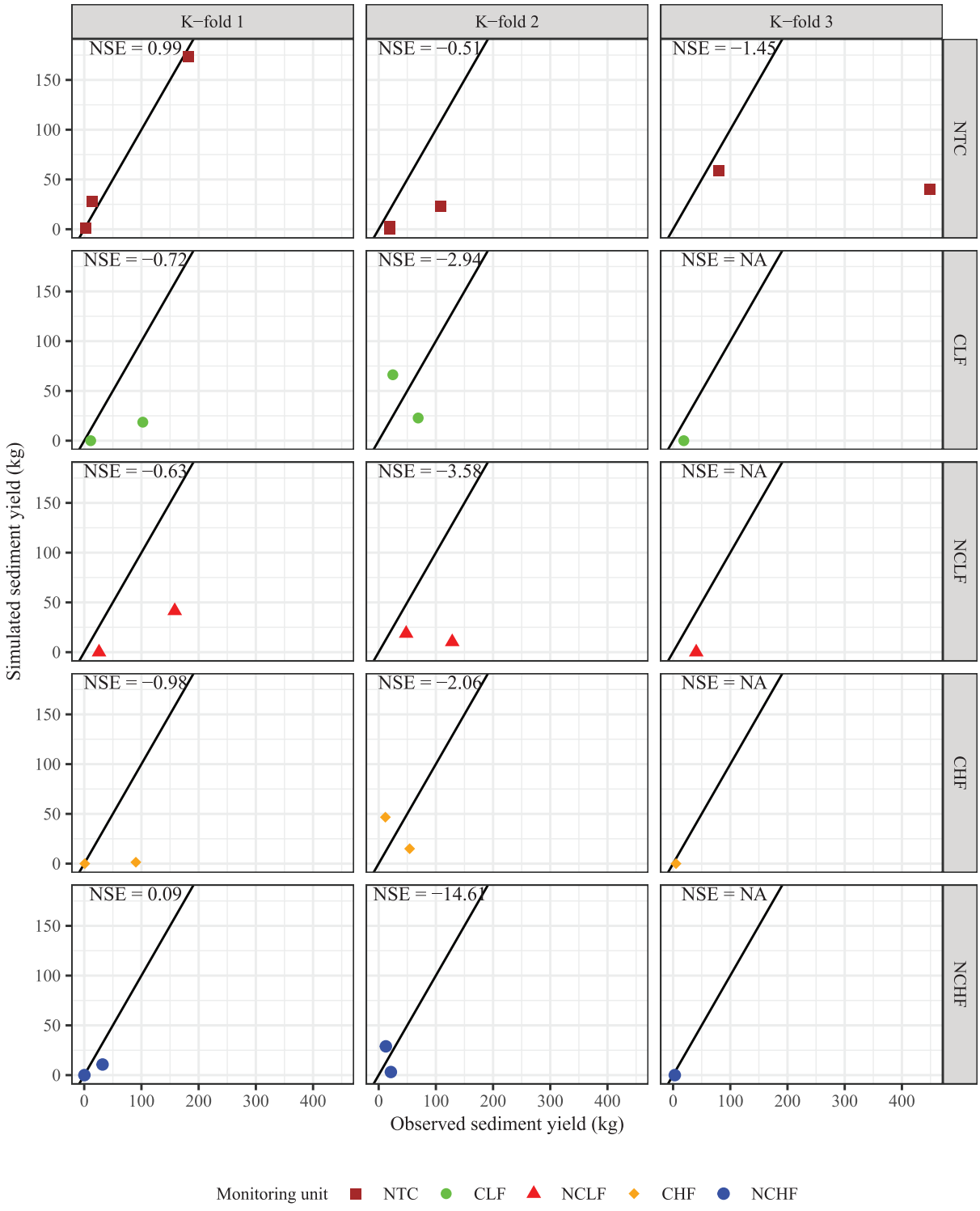

FIGURE 10 | Observed and simulated sediment yield during the validation step for each K-fold and monitoring unit. Where: the continuous line represents the plane 1:1, NTC is the no-till zero order catchment; CLF is the monitoring unit with chiselling and low phytomass amount; NCLF is the monitoring unit without chiselling and low phytomass amount; CHF is the monitoring unit with chiselling and high phytomass amount; and, NCHF is the monitoring unit without chiselling and high phytomass amount.

3.4 | Validating LISEM

The median calibrated values of K_{sat}, n, RR, coh, and coh_{veg} were used to validate the rainfall events for each K-fold (Figure 6).

Figure 8 shows the validation results for runoff volumes across K-folds and monitoring units. For the macroplots, all K-folds produced NSE values above 0.65, indicating good model performance; most exceeded 0.75, classified as very good according to Moriasi et al. (2007). However, in K-fold 3, one event (02/10/2018)

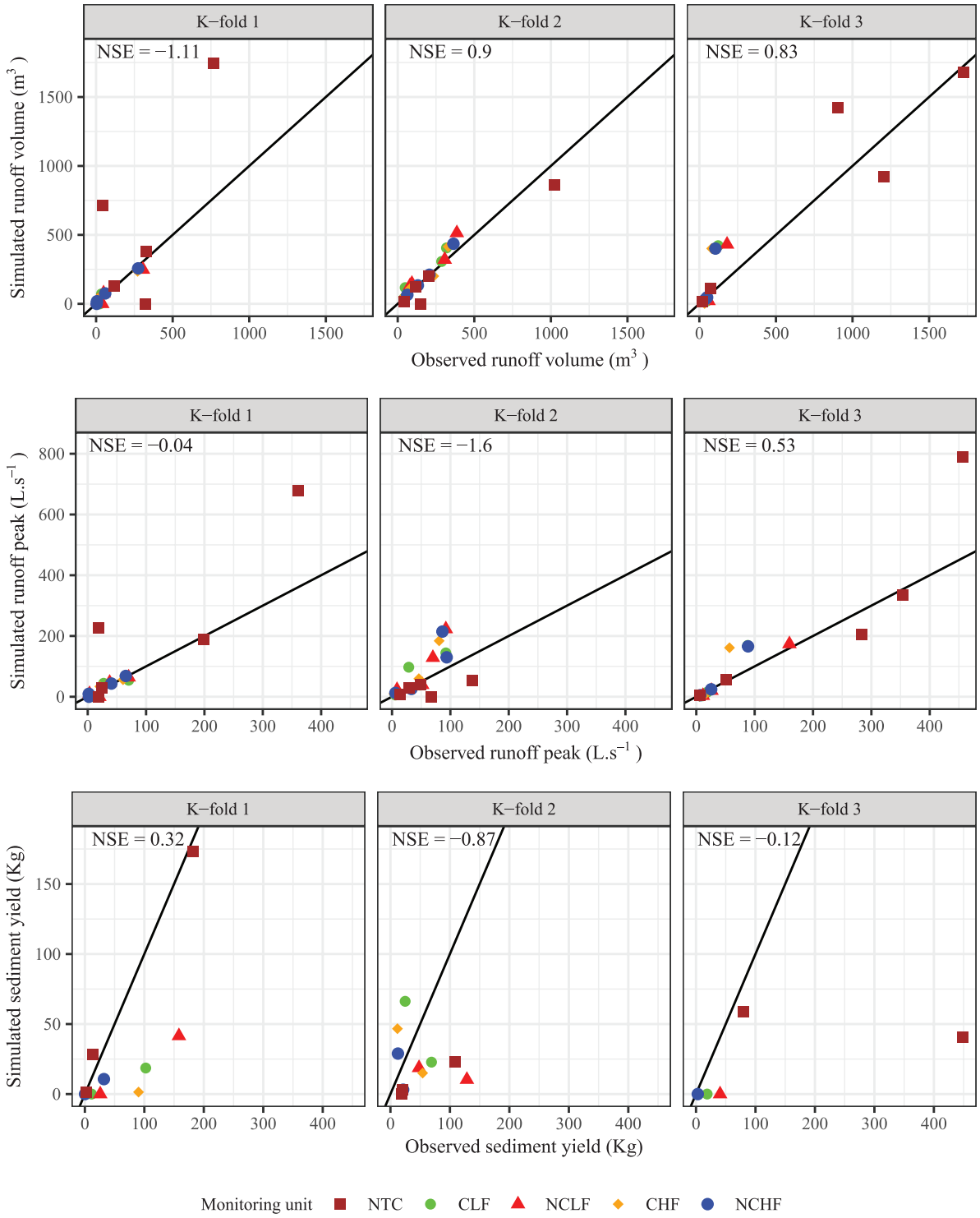

FIGURE 11 | Observed and simulated runoff volume, runoff peak, and sediment yield during the validation step for each and monitoring unit. Where: the continuous line represents the plane 1:1; NTC is the no-till zero order catchment; CLF is the monitoring unit with chiselling and with low phytomass amount; NCLF is the monitoring unit without chiselling and with low phytomass amount; CHF is the monitoring unit with chiselling and with high phytomass amount; and, NCHF is the monitoring unit without chiselling and with high phytomass amount.

diverged substantially from observed data, resulting in an unsatisfactory NSE of < 0.5. This event featured high rainfall depth and intensity, and its performance reflects the strong sensitivity of LISEM to K_{sat}: during calibration K_{sat} was twice as high as in validation. Similar findings have been reported by Jerszurki et al. (2022), who demonstrated a strong influence of K_{sat} on runoff volume, as also observed in our results, where K_{sat}, RR, and Manning's coefficient showed high sensitivity.

For the NTC, K-folds 2 and 3 produced the best fits. Poorly performing NTC events also had much higher K_{sat} values during calibration than validation, reinforcing the sensitivity of this parameter.

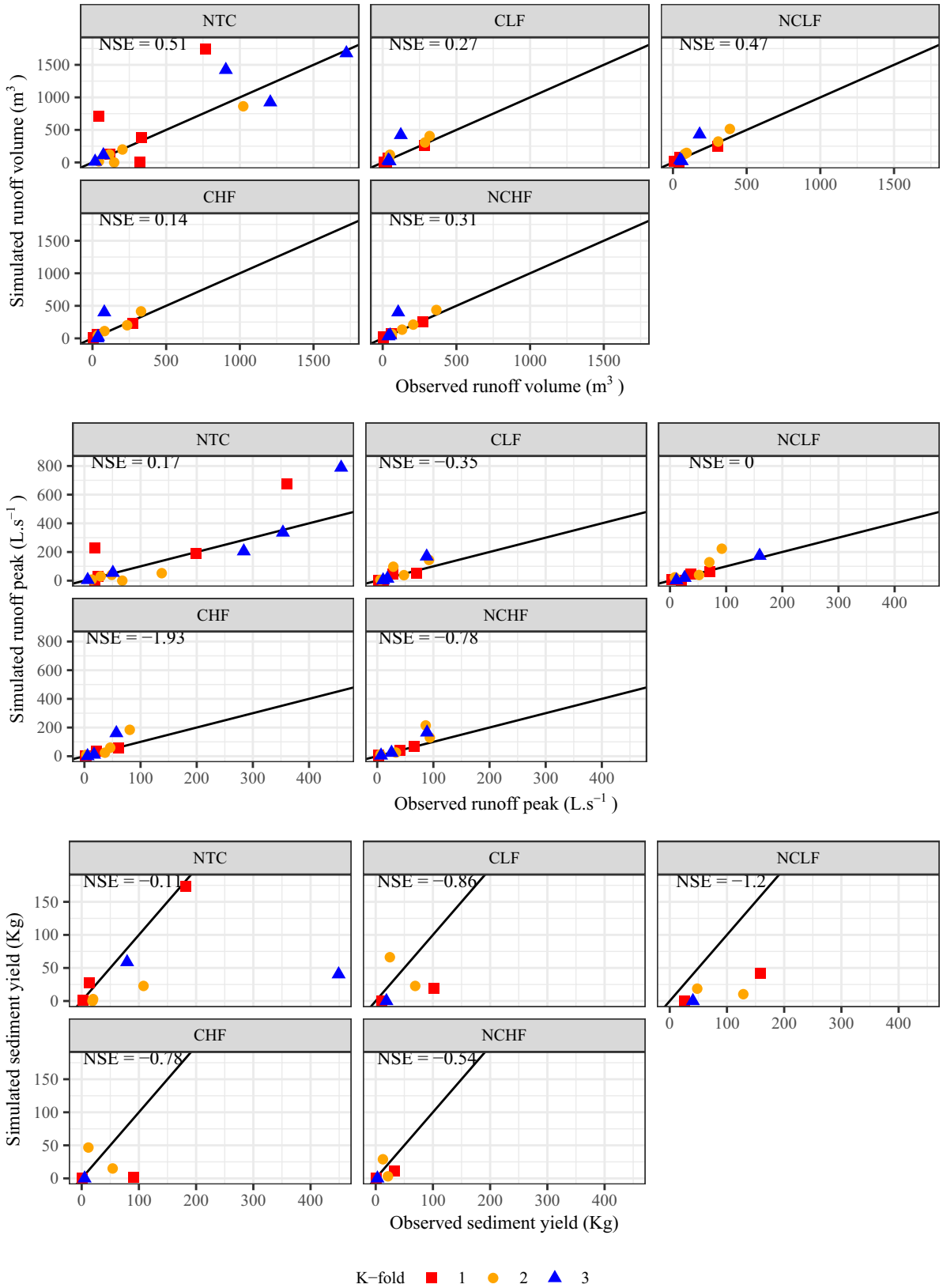

FIGURE 12 | Observed and simulated runoff volume, runoff peak, and sediment yield during the validation step for each K-fold. Where: the continuous line represents the plane 1:1, NTC is the no-till zero-order catchment; CLF is the monitoring unit with chiseling and with low phytomass amount; NCLF is the monitoring unit without chiseling and with low phytomass amount; CHF is the monitoring unit with chiseling and with high phytomass amount; and, NCHF is the monitoring unit without chiseling and with high phytomass amount.

Figure 9 presents the validation of peak runoff for each K-fold and monitoring unit. Unlike runoff volume, peak runoff did not consistently show a good fit when analyzing each K-fold and monitoring unit. In addition to K_{sat}, Manning's coefficient had a strong influence on peak runoff, as small variations in n produced significant changes in the hydrograph. As shown in Figure 6, Manning's coefficient varied substantially across K-folds, yet median values were used in the simulations. Even small changes in n can lead to substantial differences; nevertheless, most validation events still achieved satisfactory performance (NSE > 0.5).

Figure 10 presents the validation results for sediment yield. NSE values were generally unsatisfactory (NSE < 0.5), except for the NTC in K-fold 1, which showed very good performance (NSE > 0.75). Sediment yield proved to be highly sensitive to cohesion and Manning's coefficient, both of which showed considerable variation during calibration. For K-fold 3, the macroplots (CLF, NCLF, CHF, and NCHF) recorded only one event with measurable sediment yield; therefore, NSE values could not be calculated.

Figure 11 shows the observed and simulated runoff volume, peak runoff, and sediment yield for each monitoring unit during validation. When aggregating the three folds, the K-fold statistical test indicates that relationships were not consistently strong. Similar patterns appear in Figure 12: Depending on the variable, performance was better for runoff volume (K-folds 2 and 3) or peak runoff (K-fold 3), whereas none of the folds produced satisfactory results for sediment yield.

These results confirm that LISEM is highly sensitive to the parameters used in validation, particularly K_{sat}, Manning's coefficient, RR, and soil cohesion. This sensitivity reflects field reality, as these parameters exhibit spatial and temporal variability and are strongly influenced by land management. Jetten et al. (1998) also reported a strong influence of these parameters in a northern catchment in France. Likewise, Ebling et al. (2024), working in paired catchments, found that K_{sat} had to be reduced up to 50% to simulate runoff volume and sediment yield. Our findings are consistent with these studies, highlighting LISEM's strong dependence on these key parameters.

4 | Conclusions

The results of this study indicate that LISEM adequately reproduced runoff and sediment yield across all monitoring units during the calibration step. Cross-validation improved the robustness of the results by reducing calibration bias: distinct groups of events were alternately used for calibration and validation, minimizing the influence of individual events and strengthening confidence in the results. A good fit was obtained for runoff peak and runoff volume, whereas sediment yield was reproduced less satisfactorily, indicating model limitations that warrant further refinement, particularly for highly cohesive soils. Model response was strongly influenced by a small set of parameters (K_{sat}, Manning's n, RR, and soil cohesion) during calibration and validation. Further modeling studies of cohesive soils under no-till are essential to better represent soil losses.

Regarding the spatial scale, calibration performance was not negatively affected. During validation, however, the model performed better for larger scale (NTC) compared with the macroplots. This result suggests that parameter adjustments and higher variability in smaller areas can substantially influence simulation outcomes, reflecting the high sensitivity of LISEM to parameters governing infiltration, flow propagation, and erosion processes.

Chiselling did not directly impact the simulation of rainfall-runoff events, although monitoring units under chiselling presented slightly higher Manning's n, K_{sat}, and RR values. Similarly, monitoring units with greater amounts of cover crops exhibited modest increases in these parameters, yet still within the same order of magnitude as the remaining units. Seasonal variability in surface conditions under no-till affects hydrological responses and must be accounted for. Together, these findings indicate that, for this set of simulated events, LISEM shows only moderate sensitivity to chiselling and to variations in phytomass or cover crops.

The calibrated events revealed a strong relationship between apparent infiltration and LISEM-simulated infiltration, demonstrating that the model reliably represents infiltration processes at the hillslope scale.

Overall, this study highlights the importance of considering soil properties and surface cover characteristics when predicting infiltration and runoff across different environments. It also emphasizes the need for continued refinement of process-based models used to simulate infiltration and runoff, particularly for complex environments with varying surface cover, and cohesive and highly weathered soils.

Acknowledgements

This study was funded by the CAPES (Coordenação de Aperfeiçoamento de Pessoal de Nível Superior). The authors acknowledge the financial support granted by the Maiságua Project (2012–2018), FAPERGS (Fundação de Amparo à Pesquisa do Estado do Rio Grande do Sul), and CNPq (Conselho Nacional de Desenvolvimento Científico e Tecnológico). The Article Processing Charge for the publication of this research was funded by the Coordenação de Aperfeiçoamento de Pessoal de Nível Superior - Brasil (CAPES) (ROR identifier: 00x0ma614).

Funding

This work was supported by Conselho Nacional de Desenvolvimento Científico e Tecnológico. Coordenação de Aperfeiçoamento de Pessoal de Nível Superior. Fundação de Amparo à Pesquisa do Estado do Rio Grande do Sul.

Data Availability Statement

The data that support the findings of this study are available from the corresponding author upon reasonable request.

References

Almeida, W. S. d., S. Seitz, L. F. C. d. Oliveira, and D. F. d. Carvalho. 2021. "Duration and Intensity of Rainfall Events With the Same Erosivity Change Sediment Yield and Runoff Rates." *International Soil and Water Conservation Research* 9, no. 1: 69–75. https://doi.org/10.1016/j.iswcr.2020.10.004.

Alvares, C. A., J. L. Stape, P. C. Sentelhas, J. D. M. Gonçalves, and G. Sparovek. 2013. "Köppen's Climate Classification Map for Brazil." *Meteorologische Zeitschrift* 22, no. 6: 711–728. https://doi.org/10.1127/0941-2948/2013/0507.

Arabameri, A., A. Arora, S. C. Pal, et al. 2021. "K-Fold and State-of-The-Art Metaheuristic Machine Learning Approaches for Groundwater Potential Modelling." *Water Resources Management* 35, no. 6: 1837–1869. https://doi.org/10.1007/s11269-021-02815-5.

Assouline, S. 2013. "Infiltration Into Soils: Conceptual Approaches and Solutions." *Water Resources Research* 49, no. 4: 1755–1772. https://doi.org/10.1002/wrcr.20155.

Baets, S. D., D. Torri, J. Poesen, M. P. Salvador, and J. Meersmans. 2008. "Modelling Increased Soil Cohesion due to Roots With EUROSEM." *Earth Surface Processes and Landforms* 33, no. 13: 1948–1963 Portico. https://doi.org/10.1002/esp.1647.

Barbosa, F. T., I. Bertol, R. D. S. Werner, J. C. Ramos, and R. R. Ramos. 2021. "Comprimento Crítico De Declive Relacionado À Erosão Hídrica, Em Três Tipos E Doses De Resíduos Em Duas Direções De Semeadura Direta." *Revista Brasileira De Ciência do Solo* 36: 1279–1290. https://doi.org/10.1590/S0100-06832012000400022.

Barros, C. A. P., G. Govers, J. P. G. Minella, and R. Ramon. 2021. "How Water Flow Components Affect Sediment Dynamics Modeling in a Brazilian Catchment." *Journal of Hydrology* 597: 126111. https://doi.org/10.1016/j.jhydrol.2021.126111.

Bertol, I., N. P. Cogo, and E. A. Cassol. 2000. "Distância Entre Terraços Usando O Comprimento Crítico De Rampa Em Dois Preparos Conservacionistas De Solo." *Revista Brasileira de Ciência do Solo* 24: 417–425. https://doi.org/10.1590/S0100-06832000000200018.

Boddey, R. M., C. P. Jantalia, P. C. Conceiçao, et al. 2010. "Carbon Accumulation at Depth in Ferralsols Under Zero-Till Subtropical Agriculture." *Global Change Biology* 16, no. 2: 784–795. https://doi.org/10.1111/j.1365-2486.2009.02020.x.

Bradford, J. M., and C. Huang. 1994. "Interrill Soil Erosion as Affected by Tillage and Residue Cover." *Soil and Tillage Research* 31, no. 4: 353–361. https://doi.org/10.1016/0167-1987(94)90041-8.

Bronstert, A., J.-C. de Araújo, R. J. Batalla, et al. 2014. "Process-Based Modelling of Erosion, Sediment Transport and Reservoir Siltation in Mesoscale Semi-Arid Catchments." *Journal of Soils and Sediments* 14, no. 12: 2001–2018. https://doi.org/10.1007/s11368-014-0994-1.

Carson, M. A., and M. J. Kirkby. 1972. *Hillslope Form and Process*. Cambridge University Press.

Cerdan, O., Y. Le Bissonnais, A. Couturier, and N. Saby. 2002. "Modelling Interrill Erosion in Small Cultivated Catchments." *Hydrological Processes* 16, no. 16: 3215–3226. https://doi.org/10.1002/hyp.1098.

Cogo, N. P., R. Levien, and R. Schwarz. 2003. "Perdas de Solo e Água Por Erosão Hídrica Influenciadas Por Métodos de Preparo, Classes de Declive e Níveis de Fertilidade do Solo." *Revista Brasileira de Ciência do Solo* 27, no. 4: 743–753. https://doi.org/10.1590/S0100-06832003000400019.

Cogo, N. P., W. C. Moldenhauer, and G. R. Foster. 1983. "Effect of Crop Residue, Tillage-Induced Roughness, and Runoff Velocity on Size Distribution of Eroded Soil Aggregates." *Soil Science Society of America Journal* 47, no. 5: 1005–1008. https://doi.org/10.2136/sssaj1983.03615995004700050033x.

Dalla Rosa, J., M. Cooper, F. Darboux, and J. C. Medeiros. 2012. "Soil Roughness Evolution in Different Tillage Systems Under Simulated Rainfall Using a Semivariogram-Based Index." *Soil and Tillage Research* 124: 226–232. https://doi.org/10.1016/j.still.2012.06.001.

Dang, Y. P., K. L. Page, R. C. Dalal, and N. W. Menzies. 2020. "No-Till Farming Systems for Sustainable Agriculture: An Overview." *No-Till Farming Systems for Sustainable Agriculture*: 3–20. https://doi.org/10.1007/978-3-030-46409-7_1.

Dávila-Hernández, S., J. González-Trinidad, H. E. Júnez-Ferreira, et al. 2022. "Effects of the Digital Elevation Model and Hydrological Processing Algorithms on the Geomorphological Parameterization." *Water (Switzerland)* 14, no. 15: 2363. https://doi.org/10.3390/w14152363.

de Barros, C. A. P., J. P. G. Minella, L. Dalbianco, and R. Ramon. 2014. "Description of Hydrological and Erosion Processes Determined by Applying the LISEM Model in a Rural Catchment in Southern Brazil." *Journal of Soils and Sediments* 14, no. 7: 1298–1310. https://doi.org/10.1007/s11368-014-0903-7.

de Barros, C. A. P., J. P. G. Minella, R. Tassi, L. Dalbianco, and A. S. Ottonelli. 2014. "Estimativa da Infiltração de Água no Solo na Escala de Bacia Hidrográfica." *Revista Brasileira de Ciência do Solo* 38, no. 2: 557–564. https://doi.org/10.1590/S0100-06832014000200020.

De Roo, A. P. J., and V. G. Jetten. 1999. "Calibrating and Validating the LISEM Model for Two Data Sets From The Netherlands and South Africa." *Catena* 37, no. 3–4: 477–493. https://doi.org/10.1016/S0341-8162(99)00034-X.

de Vente, J., J. Poesen, M. Arabkhedri, and G. Verstraeten. 2007. "The Sediment Delivery Problem Revisited." *Progress in Physical Geography* 31, no. 2: 155–178. https://doi.org/10.1177/0309133307076485.

de Vente, J., J. Poesen, G. Verstraeten, et al. 2013. "Predicting Soil Erosion and Sediment Yield at Regional Scales: Where Do We Stand?" *Earth-Science Reviews* 127: 16–29. https://doi.org/10.1016/j.earscirev.2013.08.014.

Derpsch, R., T. Friedrich, A. Kassam, and L. Hongwen. 2010. "Current Status of Adoption of No-Till Farming in the World and Some of Its Main Benefits." *International Journal of Agricultural and Biological Engineering* 3, no. 1: 1–25. https://doi.org/10.3965/j.issn.1934-6344.2010.01.001-025.

Deuschle, D., J. P. G. Minella, T. d. A. N. Hörbe, A. L. Londero, and F. J. A. Schneider. 2019. "Erosion and Hydrological Response in No-Tillage Subjected to Crop Rotation Intensification in Southern Brazil." *Geoderma* 340 (July 2018): 157–163. https://doi.org/10.1016/j.geoderma.2019.01.010.

Didoné, E. J., J. P. Gomes Minella, and D. G. Allasia Piccilli. 2021. "How to Model the Effect of Mechanical Erosion Control Practices at a Catchment Scale?" *International Soil and Water Conservation Research* 9, no. 3: 370–380. https://doi.org/10.1016/j.iswcr.2021.01.007.

dos Santos, K. F., F. T. Barbosa, I. Bertol, R. d. S. Werner, N. H. Wolschick, and J. M. Mota. 2018. "Study of Soil Physical Properties and Water Infiltration Rates in Different Types of Land Use." *Semina: Ciências Agrárias* 39, no. 1: 87–98. https://doi.org/10.5433/1679-0359.2018v39n1p87.

Dunne, T., W. Zhang, and B. F. Aubry. 1991. "Effects of Rainfall, Vegetation, and Microtopography on Infiltration and Runoff." *Water Resources Research* 27, no. 9: 2271–2285 Portico. https://doi.org/10.1029/91wr01585.

Dymond, J. R., and S. S. Vale. 2018. "An Event-Based Model of Soil erosion and Sediment Transport at the Catchment Scale." *Geomorphology* 318: 240–249. https://doi.org/10.1016/j.geomorph.2018.06.019.

Ebling, E. D., I. Althoff, and J. M. Reichert. 2024. "Hydrosedimentology of Paired Watersheds with Clayey Soils Under Cattle Grazing and No-tillage Cropping: LISEM Calibration and Validation." *International Journal of Environmental Science and Technology* 21: 9481–9500. https://doi.org/10.1007/s13762-024-05603-x.

Engman, E. T. 1986. "Roughness Coefficients for Routing Surface Runoff." *Journal of Irrigation and Drainage Engineering* 112, no. 1: 39–53. https://doi.org/10.1061/(ASCE)0733-9437(1986)112:1(39).

Ferreira, C. J. B., C. A. Tormena, E. D. C. Severiano, L. Zotarelli, and E. Betioli Júnior. 2020. "Soil Compaction Influences Soil Physical Quality and Soybean Yield Under Long-Term No-Tillage." *Archives of Agronomy and Soil Science* 67, no. 3: 383–396. https://doi.org/10.1080/03650340.2020.1733535.

Ferreira, L. B., F. F. da Cunha, R. A. de Oliveira, and E. I. Fernandes Filho. 2019. "Estimation of Reference Evapotranspiration in Brazil With Limited Meteorological Data Using ANN and SVM – A New Approach." *Jornal of Hydrology* 572: 556–570. https://doi.org/10.1016/j.jhydrol.2019.03.028.

Fuentes-Guevara, M. D., J. Spliethoff, E. L. Camilo, et al. 2024. "Mixture of Winter Cover Crops Reduces Surface Runoff and Sediment Production Under No-Tillage System for Oxisols." *Land Degradation & Development* 35, no. 6: 2145–2156 Portico. https://doi.org/10.1002/ldr.5050.

Fuentes-Llanillo, R., T. S. Telles, D. Soares Junior, T. R. de Melo, T. Friedrich, and A. Kassam. 2021. "Expansion of No-Tillage Practice in Conservation Agriculture in Brazil." *Soil and Tillage Research* 208: 104877. https://doi.org/10.1016/j.still.2020.104877.

Govers, G., I. Takken, and K. Helming. 2000. "Soil Roughness and Overland Flow to Cite This Version: Agronomie." 20, no. 2: 131–146.

Green, W. H., and G. A. Ampt. 1911. "Studies on Soil Physics: 1. The Flow of Air and Water Through Soils." *Journal of Agricultural Science* 4, no. 1: 1–24. https://doi.org/10.1017/S0021859600001441.

Hamada, E., and H. S. Pinto. 2001. "Avaliação do Desenvolvimento do Trigo Utilizando Medidas Radiométricas em Função de Graus-Dia." Anais X Simpósio Brasileiro de Sensoriamento Remoto 95–101.

Hawkins, R. H., and T. W. Cundy. 1987. "Steady-State Analysis of Infiltration and Overland Flow for Spatially-Varied Hillslopes 1." *JAWRA Journal of the American Water Resources Association* 23, no. 2: 251–256 Portico. https://doi.org/10.1111/j.1752-1688.1987.tb00804.x.

Hessel, R., and T. van Asch. 2003. "Modelling Gully Erosion for a Small Catchment on the Chinese Loess Plateau." *Catena* 54, no. 1–2: 131–146. https://doi.org/10.1016/S0341-8162(03)00061-4.

Hessel, R., R. van den Bosch, and O. Vigiak. 2006. "Evaluation of the LISEM Soil erosion Model in Two Catchments in the East African Highlands." *Earth Surface Processes and Landforms* 31, no. 4: 469–486. https://doi.org/10.1002/esp.1280.

Horton, R. E. 1933. "The Role of Infiltration in the Hydrologic Cycle." *Eos, Transactions American Geophysical Union* 14, no. 1: 446–460. https://doi.org/10.1029/TR014i001p00446.

IUSS Working Group WRB. 2014. *World Reference Base for Soil Resources 2014: International Soil Classification System for Naming Soils and Creating Legends for Soil Maps*, World Soil Resour. Reports No. 106, 1–191. https://doi.org/10.1017/S0014479706394902.

Jerszurki, L., G. B. Schultz, D. Jerszurki, and I. dos Santos. 2022. "Sensitivity Analysis of the OpenLISEM Model: Calibration for an Unpaved Road in Southern Brazil." *Modeling Earth Systems and Environment* 8: 3089–3102. https://doi.org/10.1007/s40808-021-01288-0.

Jetten, V., A. de Roo, and J. Guérif. 1998. "Sensitivity of the Model LISEM to Variables Related to Agriculture." In *Modelling Soil Erosion by Water*, edited by J. Boardman and D. Favis-Mortlock, vol. 55, 339–349. Springer Berlin Heidelberg. https://doi.org/10.1007/978-3-642-58913-3_25.

Jetten, V., G. Govers, and R. Hessel. 2003. "Erosion Models: Quality of Spatial Predictions." *Hydrological Processes* 17, no. 5: 887–900. https://doi.org/10.1002/hyp.1168.

Julien, P. Y. 2018. *River Mechanics*. Cambridge University Press.

Kassam, A., T. Friedrich, and R. Derpsch. 2018. "Global Spread of Conservation Agriculture." *International Journal of Environmental Studies* 76, no. 1: 29–51. https://doi.org/10.1080/00207233.2018.1494927.

Koppe, E., F. J. A. Schneider, A. L. Londero, R. de Queiroz, L. Buligon, and J. P. G. Minella. 2022. "Soil Water Infiltration Evaluation From Punctual to Hillslope Scales." *Environmental Monitoring and Assessment* 194, no. 4: 300. https://doi.org/10.1007/s10661-022-09893-x.

Kværnø, S. H., and J. Stolte. 2012. "Effects of Soil Physical Data Sources on Discharge and Soil Loss Simulated by the LISEM Model." *Catena* 97: 137–149. https://doi.org/10.1016/j.catena.2012.05.001.

Le Bissonnais, Y., O. Cerdan, V. Lecomte, H. Benkhadra, V. Souchère, and P. Martin. 2005. "Variability of Soil Surface Characteristics Influencing Runoff and Interrill erosion." *Catena* 62, no. 2–3: 111–124. https://doi.org/10.1016/j.catena.2005.05.001.

Liu, J., B. A. Engel, Y. Wang, Y. Wu, Z. Zhang, and M. Zhang. 2019. "Runoff Response to Soil Moisture and Micro-Topographic Structure on the Plot Scale." *Scientific Reports* 9, no. 1: 1–13. https://doi.org/10.1038/s41598-019-39409-6.

Londero, A. L., J. P. G. Minella, F. J. A. Schneider, et al. 2021. "Quantifying the Impact of No-Till on Runoff in Southern Brazil at Hillslope and Catchment Scales." *Hydrological Processes* 35: 3. https://doi.org/10.1002/hyp.14094.

Londero, A. L., J. P. G. Minella, F. J. A. Schneider, et al. 2021. "Quantifying the Impact of No-Till on Sediment Yield in Southern Brazil at the Hillslope and Catchment Scales." *Hydrological Processes* 35, no. 7: e14286. https://doi.org/10.1002/hyp.14286.

Merten, G. H., A. G. Araújo, R. C. M. Biscaia, G. M. C. Barbosa, and O. Conte. 2015. "No-Till Surface Runoff and Soil Losses in Southern Brazil." *Soil and Tillage Research* 152: 85–93. https://doi.org/10.1016/j.still.2015.03.014.

Minella, J. P. G., D. E. Walling, and G. H. Merten. 2014. "Establishing a Sediment Budget for a Small Agricultural Catchment in Southern Brazil, to Support the Development of Effective Sediment Management Strategies." *Journal of Hydrology* 519, no. PB: 2189–2201. https://doi.org/10.1016/j.jhydrol.2014.10.013.

Morais, L. F. B., and N. P. Cogo. 2001. "Comprimentos Críticos de Rampa Para Diferentes Manejos de Resíduos Culturais em Sistema de Semeadura Direta em um Argissolo Vermelho da Depressão Central (RS)." *Revista Brasileira de Ciência do Solo* 25, no. 4: 1041–1051. https://doi.org/10.1590/S0100-06832001000400026.

Moriasi, D. N., J. G. Arnold, M. W. Van Liew, R. L. Bingner, R. D. Harmel, and T. L. Veith. 2007. "Model Evaluation Guidelines for Systematic Quantification of Accuracy in Watershed Simulations." *Transactions of the ASABE* 50, no. 3: 885–900. https://doi.org/10.13031/2013.23153.

Moriasi, D. N., M. W. Gitau, N. Pai, and P. Daggupati. 2015. "Hydrologic and Water Quality Models: Performance Measures and Evaluation Criteria." *Transactions of the ASABE* 58, no. 6: 1763–1785. https://doi.org/10.13031/trans.58.10715.

Moro, M. 2010. "Avaliação do Modelo Lisem na Simulação Dos Processos Hidrossedimentológicos de Uma Pequena Bacia Rural Localizada Nas Encostas Basálticas do Rio Grande do Sul." Universidade Federal do Rio Grande do Sul - UFRGS.

Nearing, M. A., V. Jetten, C. Baffaut, et al. 2005. "Modeling Response of Soil erosion and Runoff to Changes in Precipitation and Cover." *Catena* 61, no. 2–3: 131–154. https://doi.org/10.1016/j.catena.2005.03.007.

NRCS. 2009. *Part 650 Engineering Field Handbook. National Engineering Handbook, Chapter 2: Estimating Runoff Volume and Peak Discharge*. U.S. Department of Agriculture, Soil Conservation Service.

Pandey, A., S. K. Himanshu, S. K. Mishra, and V. P. Singh. 2016. "Physically Based Soil erosion and Sediment Yield Models Revisited." *Catena* 147: 595–620. https://doi.org/10.1016/j.catena.2016.08.002.

Pott, C. A., P. M. Conrado, L. Rampim, et al. 2023. "Mixture of Winter Cover Crops Improves Soil Physical Properties Under No-Tillage System in a Subtropical Environment." *Soil and Tillage Research* 234: 105854. https://doi.org/10.1016/j.still.2023.105854.

Qin, C., F. Zheng, G. V. Wilson, X. J. Zhang, and X. Xu. 2019. "Apportioning Contributions of Individual Rill erosion Processes and Their Interactions on Loessial Hillslopes." *Catena* 181: 104099. https://doi.org/10.1016/j.catena.2019.104099.

Ramon, R., J. P. G. Minella, G. H. Merten, C. A. P. de Barros, and T. Canale. 2017. "Kinetic Energy Estimation by Rainfall Intensity and Its Usefulness in Predicting Hydrosedimentological Variables in a Small

Rural Catchment in Southern Brazil." *Catena* 148, no. 11: 176–184. https://doi.org/10.1016/j.catena.2016.07.015.

Rauber, L. R., D. J. Reinert, P. I. Gubiani, and A. Loss. 2025. "Structure and Water Infiltration in an Ultisol Affected by Cover Crops and Seasonality." *Soil and Tillage Research* 247, no. March: 106366. https://doi.org/10.1016/j.still.2024.106366.

Rieke-Zapp, D. H., and M. A. Nearing. 2005. "Slope Shape Effects on Erosion." *Soil Science Society of America Journal* 69, no. 5: 1463–1471. https://doi.org/10.2136/sssaj2005.0015.

Romano, M. R. 2005. "Desempenho Fisiológico da Cultura de Milho Com Plantas de Arquitetura Contrastante: Parâmetros Para Modelos de Crescimento." Escola Superior de Agricultura Luiz de Queiroz.

Rose, C. W. 2004. *An Introduction to the Environmental Physics of Soil, Water and Watersheds*. Cambridge University Press.

Schick, J., I. Bertol, F. T. Barbosa, D. J. Miquelluti, and N. P. Cogo. 2017. "Water Erosion in a Long-Term Soil Management Experiment With a Humic Cambisol." *Revista Brasileira de Ciência do Solo* 41: 1–13. https://doi.org/10.1590/18069657rbcs20160383.

Schlesner, A. A. 2017. "Modelagem da Produção de Sedimentos em Bacia Hidrográfica Rural Sob Diferentes Equações de Eficiência de Desagregação do Modelo Erosivo LISEM." Universidade Federal de Santa Maria.

Shreve, E. A., and A. C. Downs. 2005. "Quality-Assurance Plan for the Analysis of Fluvial Sediment by the US Geological Survey Kentucky Water Science Center Sediment Laboratory." Geological Survey Reston Va.

Silva, C. C., J. P. G. Minella, A. Schlesner, et al. 2021. "Unpaved Road Conservation Planning at the Catchment Scale." *Environmental Monitoring and Assessment* 193: 595. https://doi.org/10.1007/s10661-021-09398-z.

Starkloff, T., and J. Stolte. 2014. "Applied Comparison of the erosion Risk Models EROSION 3D and LISEM for a Small Catchment in Norway." *Catena* 118: 154–167. https://doi.org/10.1016/j.catena.2014.02.004.

Te Chow, V., D. R. Maidment, and L. W. Mays. 1988. *Solutions Manual to Accompany Applied Hydrology*. McGraw-Hill.

Van den Putte, A., G. Govers, A. Leys, C. Langhans, W. Clymans, and J. Diels. 2013. "Estimating the Parameters of the Green–Ampt Infiltration Equation From Rainfall Simulation Data: Why Simpler is Better." *Journal of Hydrology* 476, no. 1: 332–344. https://doi.org/10.1016/j.jhydrol.2012.10.051.

Walling, D. E. 1983. "The Sediment Delivery Problem." *Journal of Hydrology* 65, no. 1–3: 209–237. https://doi.org/10.1016/0022-1694(83)90217-2.

Walling, D. E. 1999. "Linking Land Use, erosion and Sediment Yields in River Basins." *Hydrobiologia* 410: 223–240. https://doi.org/10.1023/A:1003825813091.

Werle, L., J. P. G. Minella, G. H. Merten, et al. 2025. "Modeling the Effect of Terracing on Runoff Control in a Rural Catchment in Southern Brazil." *Revista Brasileira de Ciência do Solo* 49: e0240108. https://doi.org/10.36783/18069657rbcs20240108.

Wilson, T. P., C. V. Miller, and E. A. Lechner. 2024. "Guidelines for the Use of Automatic Samplers in Collecting Surface-Water Quality and Sediment Data." Reston, VA. https://doi.org/10.3133/tm1D12.

Wolschick, N. H., I. Bertol, F. T. Barbosa, B. Bagio, and L. A. Biasiolo. 2021. "Remaining Effect of Long-Term Soil Tillage on Plant Biomass Yield and Water erosion in a Cambisol After Transition to No-Tillage." *Soil and Tillage Research* 213, no. 8: 105149. https://doi.org/10.1016/j.still.2021.105149.

Wong, T. T., and N. Y. Yang. 2017. "Dependency Analysis of Accuracy Estimates in K-Fold Cross Validation." *IEEE Transactions on Knowledge and Data Engineering* 29, no. 11: 2417–2427. https://doi.org/10.1109/TKDE.2017.2740926.

Yu, B., C. W. Rose, C. C. A. Ciesiolka, and U. Cakurs. 2000. "The Relationship Between Runoff Rate and Lag Time and the Effects of Surface Treatments at the Plot Scale." *Hydrological Sciences Journal* 45, no. 5: 709–726. https://doi.org/10.1080/02626660009492372.

Supporting Information

Additional supporting information can be found online in the Supporting Information section. **Appendix S1:** Online Appendix.